nature immunology

CD69 controls the uptake of L-tryptophan through LAT1-CD98 and AhR-dependent secretion of IL-22 in psoriasis

Danay Cibrian[1], María Laura Saiz[1], Hortensia de la Fuente[1], Raquel Sánchez-Díaz[2], Olga Moreno-Gonzalo[1], Inmaculada Jorge[2], Alessia Ferrarini[2], Jesús Vázquez[2], Carmen Punzón[3], Manuel Fresno[3], Miguel Vicente-Manzanares[1], Esteban Daudén[4], Pedro M Fernández-Salguero[5], Pilar Martín[2] & Francisco Sánchez-Madrid[1,2]

The activation marker CD69 is expressed by skin γδ T cells. Here we found that CD69 controlled the aryl hydrocarbon receptor (AhR)-dependent secretion of interleukin 22 (IL-22) by γδ T cells, which contributed to the development of psoriasis induced by IL-23. CD69 associated with the aromatic-amino-acid-transporter complex LAT1-CD98 and regulated its surface expression and uptake of L-tryptophan (L-Trp) and the intracellular quantity of L-Trp-derived activators of AhR. *In vivo* administration of L-Trp, an inhibitor of AhR or IL-22 abrogated the differences between CD69-deficient mice and wild-type mice in skin inflammation. We also observed LAT1-mediated regulation of AhR activation and IL-22 secretion in circulating $V_\gamma9^+$ γδ T cells of psoriatic patients. Thus, CD69 serves as a key mediator of the pathogenesis of psoriasis by controlling LAT1-CD98-mediated metabolic cues.

Psoriasis is one of the most common chronic inflammatory skin diseases, affecting about 2% of the population worldwide[1]. It is defined by a thickened epidermis (acanthosis) caused by keratinocyte proliferation and massive infiltration of leukocytes into the skin. Psoriatic lesions contain larger amounts of the pro-inflammatory cytokines interleukin 17 (IL-17), IL-21, IL-22 and IL-23, which has led to the classification of psoriasis as a disease mediated by IL-17-producing helper T cells (T_H17 cells)[2]. The importance of IL-23 and IL-17 in psoriatic patients is demonstrated by the efficacy of treatment with monoclonal antibodies to IL-17 and to the cytokine receptor IL-23R[3]. Furthermore, intradermal administration of recombinant IL-23 to mice induces a psoriasiform dermatitis that mimics the human disease in histological and immunological aspects[4].

In addition to IL-17, IL-22 also acts as a master regulator of psoriasis[5–7]. Polymorphisms in *IL22* result in enhanced susceptibility to psoriasis[8], and serum concentrations of IL-22 positively correlate with disease severity and negatively correlate with responsiveness to therapy[9]. IL-22 signaling in keratinocytes induces expression and phosphorylation of the transcription factor STAT3, which increases epidermal proliferation and de-differentiation[10]. IL-22 expression is regulated by the ligand-dependent transcription factor AhR in T_H17 cells and some populations of γδ T cells[11] and innate lymphocytes[12]. Currently described endogenous ligands for AhR also include naturally occurring dietary substances, such as L-tryptophan (L-Trp)-derived metabolites[13]. After being exposed to light, L-Trp can be metabolized to several products, including the high-affinity AhR agonist FICZ (6-formylindolo [3, 2-b] carbazole). A light-independent, H_2O_2-dependent pathway for the systemic generation of FICZ from L-Trp has also been described[14]. Uptake of aromatic amino acids by activated lymphoid cells is conducted mainly via the system L1 transporter, an heterodimer comprising the heavy chain CD98 (also known as SLC3A2 or 4F2) and the light chain LAT1 ('L-type amino acid transporter 1'; also known as SLC7A5). Regulation of amino acid transport through the LAT1-CD98 heterodimer is linked to T cell–activation and T cell–differentiation processes[15].

Although T_H17 cells were once considered an important source of IL-17 and IL-22 in psoriatic skin, evidence now indicates that these cytokines are produced mainly by a population of dermal γδ T cells already identified in both humans and mice[16–19]. Skin γδ T cells bear several markers of memory and effector T cells, including CD69 (ref. 20). Lymphocytes from CD69-deficient mice show enhanced differentiation toward the T_H17 lineage[21], and CD69-deficient mice exhibit increased severity of T_H17 cell–mediated inflammatory diseases, including collagen II–induced arthritis[22], allergic asthma and skin contact hypersensitivity[23], autoimmune myocarditis[24] and colitis[25]. Whether CD69 exerts an immunomodulatory effect on psoriasis by controlling IL-17 and IL-22 responses in skin γδ T cells has remained unexplored until now.

In this study we found that CD69-deficient mice developed an attenuated skin inflammatory response to the administration of

[1]Immunology Service, Hospital de la Princesa, Universidad Autónoma de Madrid, Instituto Investigación Sanitaria Princesa, Madrid, Spain. [2]Department of Vascular Biology and Inflammation, Centro Nacional de Investigaciones Cardiovasculares, Madrid, Spain. [3]Department of Molecular Biology, Centro de Biología Molecular Severo Ochoa, Universidad Autónoma de Madrid, Madrid, Spain. [4]Dermatology Service, Hospital de la Princesa, Madrid, Spain. [5]Department of Biochemistry, Molecular Biology and Genetic, Faculty of Sciences, University of Extremadura, Badajoz, Spain. Correspondence should be addressed to F.S.-M. (fsmadrid@salud.madrid.org).

Received 4 March; accepted 1 June; published online 4 July 2016; corrected online 11 July 2016 (details online); doi:10.1038/ni.3504

IL-23, with decreased expression of IL-22 and STAT3 in the epidermis. We also found that CD69 associated with the heterodimeric amino-acid transporter LAT1-CD98 and regulated the uptake of L-Trp. This promoted the AhR-induced secretion of IL-22 by skin γδ T cells.

RESULTS

IL-23-induced psoriasiform inflammation requires CD69

To assess the role of CD69 in psoriasis, we administered consecutive intradermal injections of mouse IL-23 protein into the ears of wild-type and CD69-deficient mice. IL-23 induced more swelling, epidermal acanthosis, dermal inflammation and keratinocyte proliferation (Ki67$^+$ nuclei) in the ears of wild-type mice than in those of CD69-deficient mice (**Fig. 1a–c**). IL-23 also significantly increased the total number of CD45$^+$ cells in wild-type mice relative to that in CD69-deficient mice (**Fig. 1d**). These were mostly CD45$^+$CD11c$^-$CD11b$^+$ myeloid (non-dendritic) cells, particularly Gr-1$^+$F4/80$^-$neutrophils, F4/80^{lo} monocytes and F4/80^{hi} macrophages (**Fig. 1d**). Immunohistochemistry also revealed more Ly6G$^+$ neutrophils and F4/80$^+$ monocytes and macrophages in wild-type mice than in CD69-deficient mice after treatment with IL-23 (**Fig. 1c**) These results indicated that the absence of CD69 prevented the development of psoriasis after intradermal injection of IL-23.

Reduced expression of IL-22 and STAT3 in CD69 deficiency

We next determined whether CD69 controls the expression of inflammatory mediators in the skin. IL-23 induced higher expression of *Cxcl1*, *S100a8* and *S100a9* mRNA in wild-type mice than in CD69-deficient mice, while both genotypes showed a similar increase in *Ccl20* mRNA (**Fig. 2a**). IL-23 treatment increased the expression of *Il6*, *Tnf*, *Il1b* and IL-17 mRNA to a similar extent in wild-type mice and CD69-deficient mice, while the expression of *Tgfb* mRNA in the skin was not altered (**Fig. 2b**,**c**). In contrast, IL-23 induced a very modest increase in IL-22 expression in the skin of CD69-deficient relative to that in the skin of wild-type mice (**Fig. 2d**). Neither genotype showed detectable expression of IL-22 or IL-17 in CD4$^+$ T cells obtained from the ear-draining lymph nodes of mice given injection of IL-23, followed by re-stimulation of the cells *in vitro* (data not shown). These results indicated that the weak

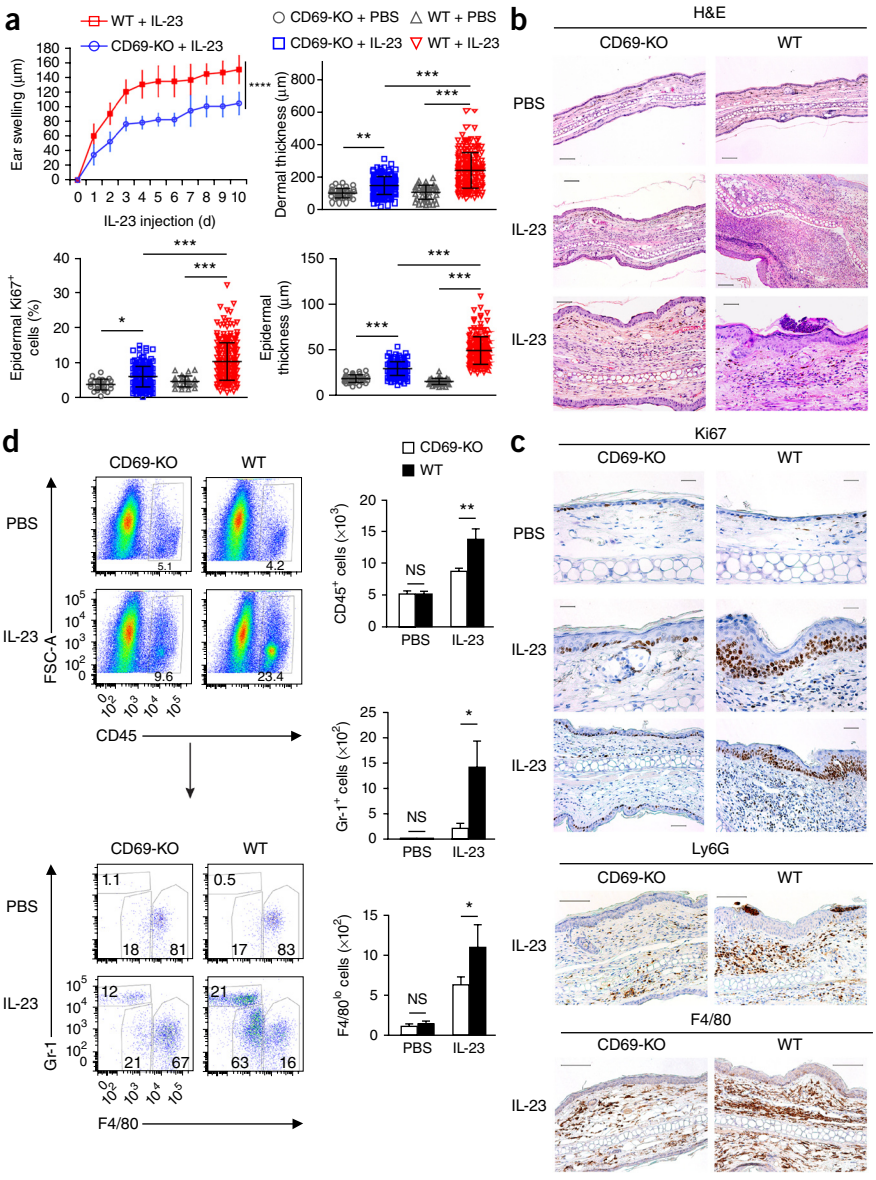

Figure 1 CD69-deficient mice develop a mild form of IL-23-induced psoriasis. (**a**) Ear thickness of CD69-deficient (CD69-KO) and wild-type (WT) mice after each intradermal injection of IL-23 (horizontal axis) (top left), and dermal and epidermal thickness and quantification of Ki67$^+$ nuclei in histological sections of ears from CD69-deficient and wild-type mice after ten doses of IL-23 (top right and bottom row). Each symbol (top right and bottom row) represents an individual image; small horizontal lines indicate the mean (± s.d.). (**b**) Hematoxylin-and-eosin (H&E)-stained sections of ear skin from CD69-deficient and wild-type mice treated with PBS or IL-23 (left margin). Scale bars, 100 μm (top and middle) or 50 μm (bottom); original magnification, ×10 (top and middle) or ×20 (bottom). (**c**) Immunohistochemistry of Ki67, Ly6G and F4/80 (above images) in the skin of CD69-deficient and wild-type mice treated with PBS or IL-23 (left margin). Scale bars, 25 μm (top and second row), 50 μm (third row) or 100 μm (bottom two rows); original magnification, ×40 (top and second row) or ×20 (bottom three rows). (**d**) Flow cytometry (left) of cells that infiltrated the ears of CD69-deficient and wild-type mice (above plots) given ten doses of PBS or IL-23 (left margin). Numbers adjacent to outlined areas indicate percent of CD45$^+$ cells among live gated cells (top group), or Gr-1$^+$ granulocytes (top left), F4/80^{lo} cells (bottom left) or F4/80^{hi} monocytes and macrophages (bottom right) among CD45$^+$CD11b$^+$CD11c$^-$ live gated cells. Right, quantification of the populations gated at left (per 1×10^4 live gated cells). FSC, forward scatter. NS, not significant ($P > 0.05$); $^*P < 0.05$, $^{**}P < 0.01$, $^{***}P < 0.001$ and $^{****}P < 0.0001$ (unpaired *t*-test (**a**, top left), one-way analysis of variance (ANOVA) with Newman-Keuls multiple-comparisons post-test (**a**, top right and bottom row) or two-way ANOVA with Bonferroni's multiple-comparisons test (**d**, right)). Data are representative of three experiments (mean ± s.d. (**a**, top left) or mean + s.e.m. (**d**); $n = 5$ mice per group).

cutaneous inflammatory response to IL-23 injection observed in the CD69-deficient mice might have been related to attenuated skin production of IL-22.

Expression of the cytokine receptor IL-22R in skin is restricted to non-hematopoietic cells, such as keratinocytes and fibroblasts. In these cells, the binding of IL-22 to IL-22R activates STAT3 (ref. 26). Injections of IL-23 into the ear caused a uniform increase in epidermal STAT3 expression and phosphorylation (at Ser727 and Tyr705) in wild-type mice, compared with only patchy induction of these parameters in CD69-deficient mice (**Fig. 2e**,**f**). This indicated that CD69 controlled the expression of IL-22 and STAT3.

Enhancement of the expression of AhR and IL-22 by CD69

CD69 is a negative regulator of the secretion of IL-17 by T_H17 cells[27], but its effect on IL-22 secretion is not known. This is a crucial question, since IL-22 is produced by T_H17 lymphocytes[13]. Naive $CD4^+$ T cells from CD69-deficient mice polarized for 48 h *in vitro* into T_H17 cells secreted less IL-22 than did their wild-type counterparts (**Supplementary Fig. 1a**). Moreover, flow cytometry after intracellular staining showed that CD69-deficient T_H17 cells had lower expression of AhR than that of wild type T_H17 cells (**Supplementary Fig. 1b**). We found that expression of mRNA from the AhR target genes *Il22*, *Ahr*, *Ahrr*, *Cyp1a* and *Cyp1b* was impaired in CD69-deficient T_H17 cells relative to that in wild-type T_H17 cells (**Supplementary Fig. 1c**).

In IL-23-driven psoriasis, IL-22 and IL-17 are secreted by dermal γδ T cells[16,18]. To characterize the resident T cell populations in the skin of both wild-type mice and CD69-deficient mice, we analyzed total skin-cell suspensions and separated dermal and epidermal layers by flow cytometry. These experiments indicated that $CD3^{hi}$ cells were dendritic epidermal γδ T cells, while 50–80% of dermal $CD3^{lo}$ cells were γδ T cells (**Supplementary Fig. 1d**). Both $CD3^{hi}$ γδ T cell populations and $CD3^{lo}$ γδ T cell populations in untreated skin had high expression of CD69 (**Supplementary Fig. 1e**). Although CD69 expression is linked to the generation and migration of skin-resident memory T cells[28], the frequency of skin-resident epidermal ($CD3^{hi}$) and dermal ($CD3^{lo}$) γδ T cell populations was similar in wild-type mice and CD69-deficient mice (**Supplementary Fig. 1f**).

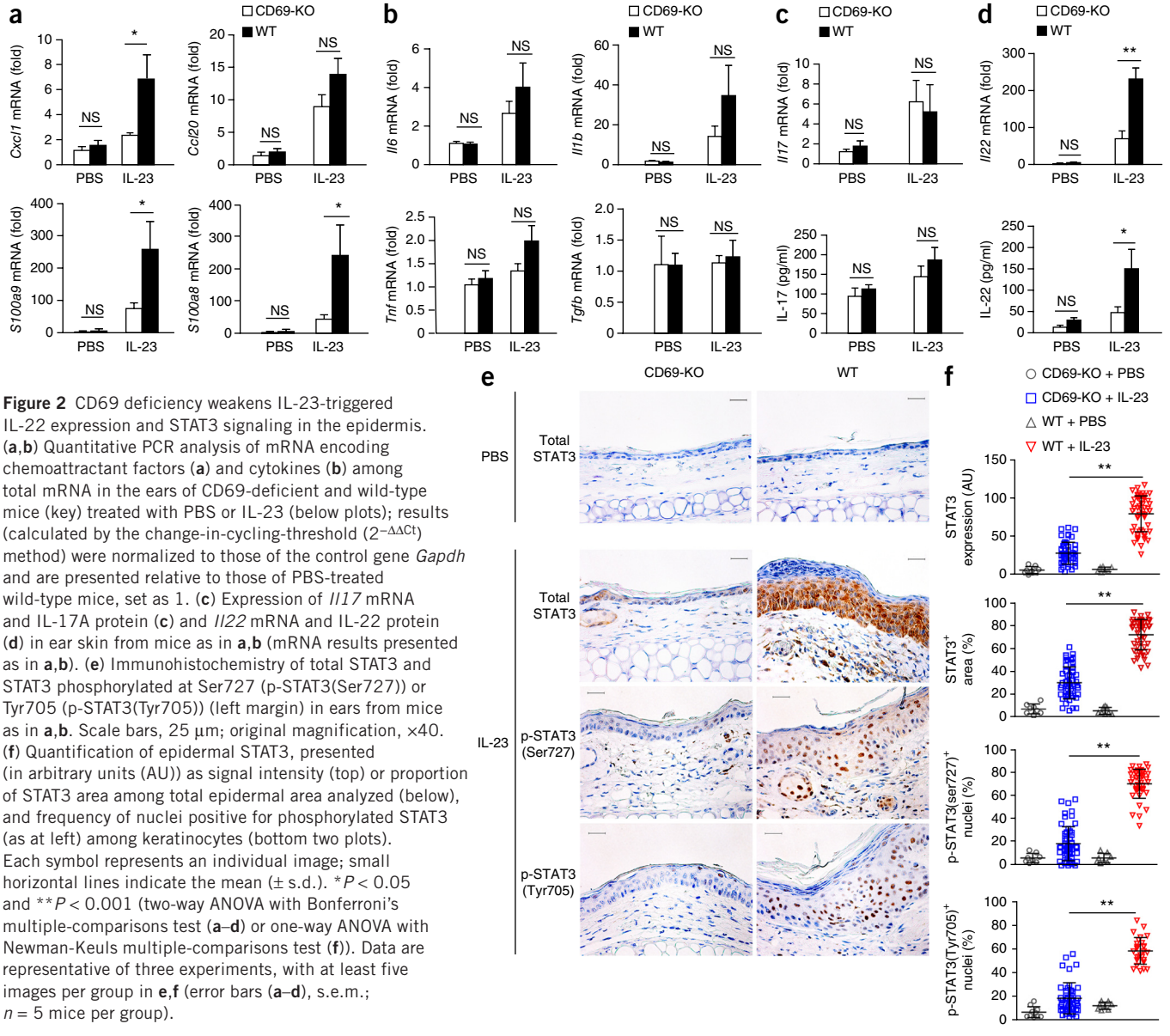

Figure 2 CD69 deficiency weakens IL-23-triggered IL-22 expression and STAT3 signaling in the epidermis. (**a**,**b**) Quantitative PCR analysis of mRNA encoding chemoattractant factors (**a**) and cytokines (**b**) among total mRNA in the ears of CD69-deficient and wild-type mice (key) treated with PBS or IL-23 (below plots); results (calculated by the change-in-cycling-threshold ($2^{-\Delta\Delta Ct}$) method) were normalized to those of the control gene *Gapdh* and are presented relative to those of PBS-treated wild-type mice, set as 1. (**c**) Expression of *Il17* mRNA and IL-17A protein (**c**) and *Il22* mRNA and IL-22 protein (**d**) in ear skin from mice as in **a**,**b** (mRNA results presented as in **a**,**b**). (**e**) Immunohistochemistry of total STAT3 and STAT3 phosphorylated at Ser727 (p-STAT3(Ser727)) or Tyr705 (p-STAT3(Tyr705)) (left margin) in ears from mice as in **a**,**b**. Scale bars, 25 µm; original magnification, ×40. (**f**) Quantification of epidermal STAT3, presented (in arbitrary units (AU)) as signal intensity (top) or proportion of STAT3 area among total epidermal area analyzed (below), and frequency of nuclei positive for phosphorylated STAT3 (as at left) among keratinocytes (bottom two plots). Each symbol represents an individual image; small horizontal lines indicate the mean (± s.d.). $*P < 0.05$ and $**P < 0.001$ (two-way ANOVA with Bonferroni's multiple-comparisons test (**a**–**d**) or one-way ANOVA with Newman-Keuls multiple-comparisons test (**f**)). Data are representative of three experiments, with at least five images per group in **e**,**f** (error bars (**a**–**d**), s.e.m.; $n = 5$ mice per group).

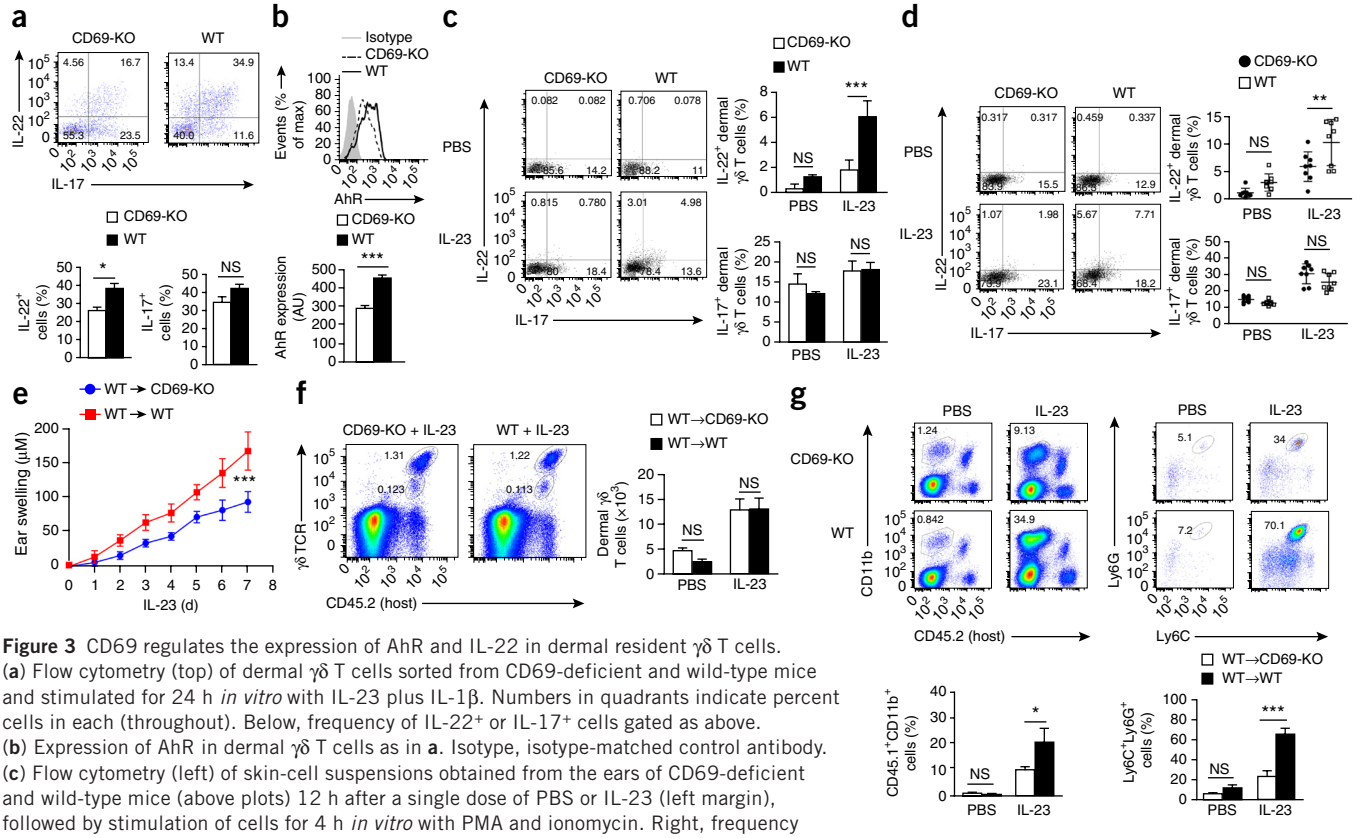

Figure 3 CD69 regulates the expression of AhR and IL-22 in dermal resident γδ T cells. (**a**) Flow cytometry (top) of dermal γδ T cells sorted from CD69-deficient and wild-type mice and stimulated for 24 h *in vitro* with IL-23 plus IL-1β. Numbers in quadrants indicate percent cells in each (throughout). Below, frequency of IL-22$^+$ or IL-17$^+$ cells gated as above. (**b**) Expression of AhR in dermal γδ T cells as in **a**. Isotype, isotype-matched control antibody. (**c**) Flow cytometry (left) of skin-cell suspensions obtained from the ears of CD69-deficient and wild-type mice (above plots) 12 h after a single dose of PBS or IL-23 (left margin), followed by stimulation of cells for 4 h *in vitro* with PMA and ionomycin. Right, frequency of IL-22$^+$ or IL-17$^+$ cells gated as at left ($n = 8$ mice per group). (**d**) Flow cytometry (left) of cells obtained from CD69-deficient and wild-type mice (above plots) 12 h after injection of a single dose of PBS and brefeldin A or IL-23 and brefeldin A (left margin). Right, frequency of IL-22$^+$ or IL-17$^+$ cells gated as at left. Each symbol represents an individual mouse ($n = 8$ per group); small horizontal lines indicated the mean (± s.d.). (**e**) Ear thickness of lethally irradiated CD69-deficient and wild-type host mice (CD45.2$^+$) reconstituted by intravenous injection of wild-type whole bone marrow cells (CD45.1$^+$) for 2 months, then given seven doses of PBS or IL-23 intradermally (assessed after each dose; horizontal axis). (**f**) Flow cytometry (left) analyzing dermal γδ T cells in CD69-deficient or wild-type (CD45.2$^+$) host chimeric mice as in **e**. Numbers adjacent to outlined areas indicate percent CD45.2$^+$ (host-resident) dermal or epidermal γδ T cells identified by high expression (top right; epidermal) or low expression (bottom right; dermal) of the γδ TCR. Right, quantification of total dermal γδ T cells (per ear) in host mice as at left after intradermal treatment with PBS or IL-23 (horizontal axis). (**g**) Flow cytometry (top) of cells from mice as in **e**. Numbers adjacent to outlined areas indicate percent CD45.1$^+$CD11b$^+$ cells among live cells (left group) or Ly6G$^+$Ly6C$^+$ cells among CD45.1$^+$CD11b$^+$F4/80$^-$ gated cells (right group). Bottom, frequency of CD45.1$^+$CD11b$^+$ and CD45.1$^+$CD11b$^+$F480$^-$Ly6G$^+$Ly6C$^+$ cells as above. *$P < 0.05$, **$P < 0.01$ and ***$P < 0.001$ (unpaired *t*-test (**a**,**b**) or two-way ANOVA and Bonferroni's multiple-comparisons test (**c**,**d**,**f**,**g**)). Data are representative of three experiments (**a**,**b**; mean + s.e.m.; $n = 3$ or 4 mice per experiment), one experiment (**c**,**d**; mean + s.d. of $n = 8$ mice per group in **c**) or two experiments (**e**–**g**; mean + s.e.m. of $n = 5$ mice per group).

Simultaneous intradermal injection of IL-23 (into the ears) and systemic (intraperitoneal) administration of the secretion inhibitor brefeldin A to wild-type mice promoted the accumulation of IL-22 in dermal CD3^{lo} γδ T cells (**Supplementary Fig. 2a**). Moreover, flow cytometry of dermal γδ T cells sorted from wild-type mice and stimulated *in vitro* with IL-23 plus IL-1β revealed an acute peak of IL-22 (maximal at 24 h after stimulation) and higher AhR expression than that of unstimulated cells (**Supplementary Fig. 2b**). However, the secretion of IL-17 from sorted dermal γδ T cells was sustained for up to 72 h after stimulation (**Supplementary Fig. 2b**).

Sorted CD69-deficient dermal γδ T cells released less IL-22 than did wild-type dermal γδ T cells when stimulated with IL-23 and IL-1β *in vitro*, whereas their IL-17 production was similar (**Fig. 3a**). Moreover, the expression of AhR induced by IL-23 and IL-1β *in vitro* stimulation was lower in CD69-deficient dermal γδ T cells than in wild-type dermal γδ T cells (**Fig. 3b**).

To parse the function of CD69 in IL-22 secretion by dermal γδ T cells *in vivo*, we prepared skin-cell suspensions 12 h after the administration of a single dose of IL-23 into the ears of wild-type and CD69-deficient mice, followed by stimulation of the cell suspensions with the phorbol ester PMA and ionomycin. Flow cytometry showed lower IL-22 expression in CD69-deficient dermal γδ T cells than in wild-type dermal γδ T cells (**Fig. 3c**). Simultaneous intradermal injection of IL-23 and intraperitoneal administration of brefeldin A resulted in lower expression of IL-22 in dermal γδ T cells from CD69-deficient mice than in those from wild-type mice (**Fig. 3d**).

We observed a similar expression of the transcription factor RORγt in dermal γδ T cells from CD69-deficient and those from wild-type mice (**Supplementary Fig. 2c**). Likewise, phosphorylation of STAT3 and STAT5 following stimulation with IL-23 plus IL-1β was similar in CD69-deficient dermal γδ T cells and wild-type dermal γδ T cells (**Supplementary Fig. 2c**). Flow cytometry of skin suspensions from mice with sequence encoding green fluorescent protein (GFP) reporter knocked into the gene encoding IL-23R[29] showed that dermal γδ T cells (CD3^{lo}) were the main population among IL-23R$^+$ (GFP$^+$) cells in the skin at steady state, while epidermal γδ T cells (CD3^{hi}) were IL-23R$^-$ (GFP$^-$) (**Supplementary Fig. 2d**). Staining of IL-23R showed that the number of IL-23R$^+$ dermal γδ T cells and their molecular density of IL-23R were similar for CD69-deficient mice and wild-type mice (**Supplementary Fig. 2e**).

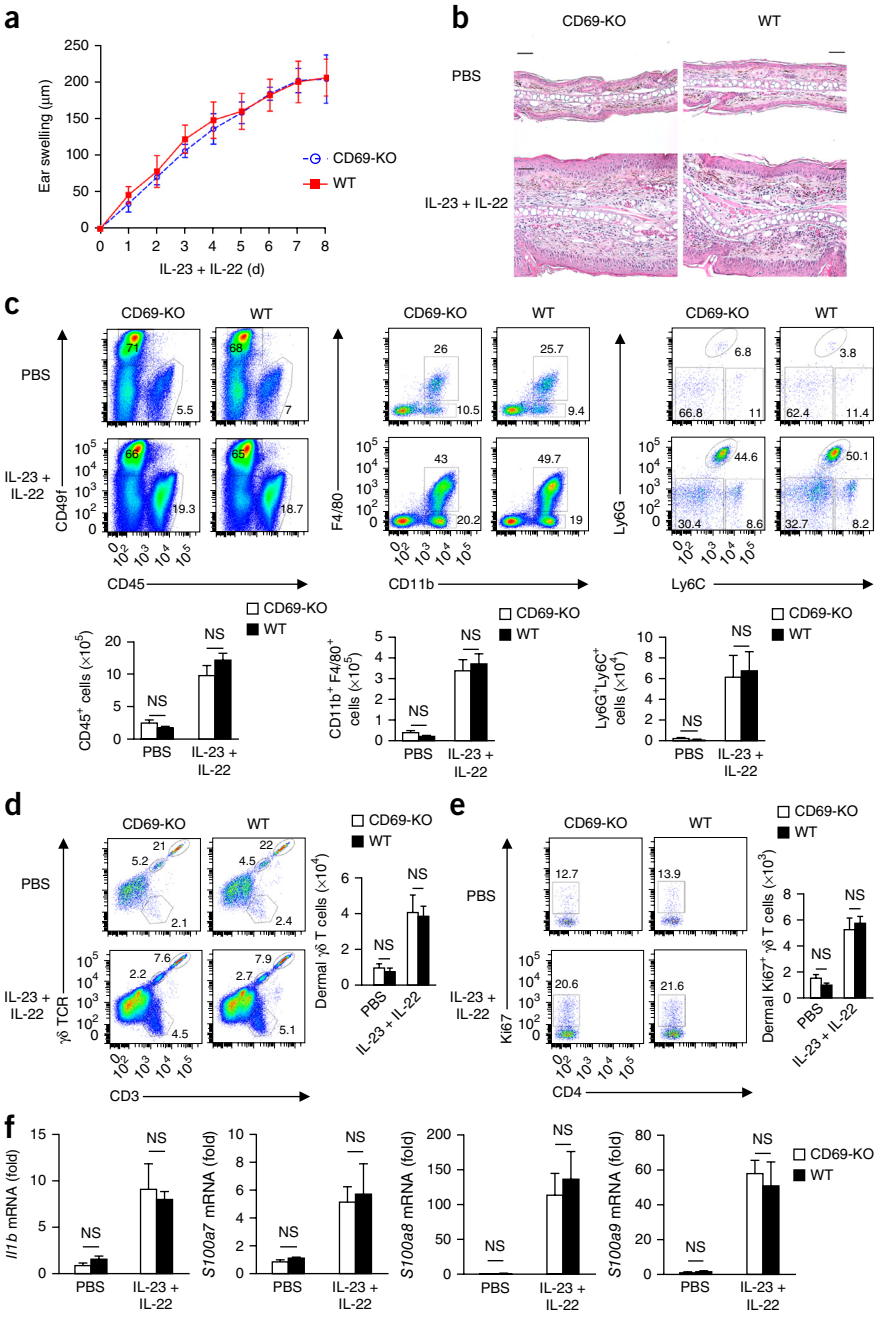

Figure 4 IL-22 mediates skin inflammation downstream of CD69. (**a**) Ear thickness of CD69-deficient and wild-type mice during the administration of eight doses of IL-23 plus IL-22 (500 ng of each; horizontal axis). (**b**) H&E-stained sections of ears from wild-type and CD69-deficient mice (above plots) treated with eight doses of PBS or with IL-23 plus IL-22 (left margin). Scale bars, 50 μm; original magnification, ×20. (**c**) Flow cytometry (top) of cells in skin suspensions from mice as in **a**. Numbers adjacent to outlined areas indicate percent CD49f$^+$CD45$^-$ keratinocytes (top left) or CD49f$^-$CD45$^+$ cells (bottom right) among live gated cells (left group), CD11b$^+$F4/80$^+$ macrophages (top) or CD11b$^+$F4/80$^-$ cells (bottom) among CD45$^+$CD11c$^-$ live gated cells (middle group), or Ly6G$^+$Ly6C$^+$ neutrophils (top), Ly6G$^-$Ly6C$^-$ cells (bottom left) or Ly6G$^-$Ly6C$^+$ cells (bottom right) among live CD45$^+$ CD11b$^+$F4/80$^-$ gated cells (right group). Below, total CD45$^+$ cells, macrophages and neutrophils (per ear) in mice as above. (**d**) Flow cytometry (left) of skin suspensions from mice as in **a**. Numbers adjacent to outlined areas indicate percent γδTCR$^-$CD3$^+$ T cells (bottom), γδTCR$^+$CD3$^+$ dermal T cells (top right) and γδTCR^{++}CD3^{++} epidermal T cells (top left) among live CD45$^+$ gated cells. Right, total dermal γδ T cells (per ear) in mice as at left. (**e**) Flow cytometry (left) of skin suspensions from mice as in **a**. Numbers adjacent to outlined areas indicate percent Ki67$^+$ cells among CD45$^+$CD3^{lo}γδTCR^{lo} gated cells. Right, total dermal Ki67$^+$ γδ T cells as at left. (**f**) Quantitative PCR analysis of *Il1b*, *S100a7*, *S100a8* and *S100a9* mRNA in the skin of mice as in **a** (presented as in **Fig. 2a**,**b**). *P* values (NS), unpaired *t*-test (**a**) or two-way ANOVA followed by Bonferroni's multiple-comparisons test (**c**–**f**). Data are representative of two independent experiments with similar results (mean ± s.d. (**a**) or mean + s.e.m. (**c**–**f**); $n = 5$ mice per group in each experiment).

CD69 is known to modulate the trafficking of effector T cells[30]. To investigate whether CD69-mediated egress of lymphocytes from the lymph node was involved in the IL-23 skin-inflammation model, we transferred wild-type (CD45.1$^+$) whole bone marrow cells intravenously into lethally γ-irradiated CD69-deficient or wild-type (CD45.2$^+$) host mice (**Fig. 3e**). After 2 months of reconstitution, we administered IL-23 intradermally to the mice. CD69-deficient host mice displayed less skin inflammation than that of wild-type host mice (**Fig. 3e**). Flow cytometry of skin-cell suspensions showed a similar increase in host-derived (CD45.2$^+$) dermal γδ T cells in CD69-deficient mice and wild-type host mice after treatment with IL-23 (**Fig. 3f**). We observed significantly more infiltrating CD11b$^+$ myeloid cells and Ly6G$^+$Ly6C$^+$ neutrophils of donor (CD45.1$^+$) origin in the skin of wild-type mice than in that of CD69-deficient mice (**Fig. 3g**). Because skin-resident dermal γδ T cells are radioresistant and proliferate *in situ*[20], they persisted in the bone-marrow-chimeric hosts, which would account for the differences between the wild-type hosts and CD69-deficient hosts. These observations ruled out the possibility of a role for the migration of CD69$^+$ T lymphocytes from the lymph nodes as a triggering mechanism.

IL-22- and AhR-mediated skin inflammation downstream of CD69

To address whether the attenuated skin inflammation observed in CD69-deficient mice was due to reduced secretion of IL-22 from the skin, we simultaneously injected IL-22 and IL-23 intradermally into wild-type mice and CD69-deficient mice. We observed a similar degree of ear swelling in mice of each genotype (**Fig. 4a**), as well as substantial acanthosis (**Fig. 4b**) and similar infiltration of myeloid cells into the skin (**Fig. 4c**), proliferation of dermal γδ T cells (**Fig. 4d**,**e**), and expression of *Il1b* and IL-22-related genes, such *S100a7*, *S100a8* and *S100a9*, in mice of each genotype (**Fig. 4f**). Moreover, intradermal injection of IL-22 alone induced

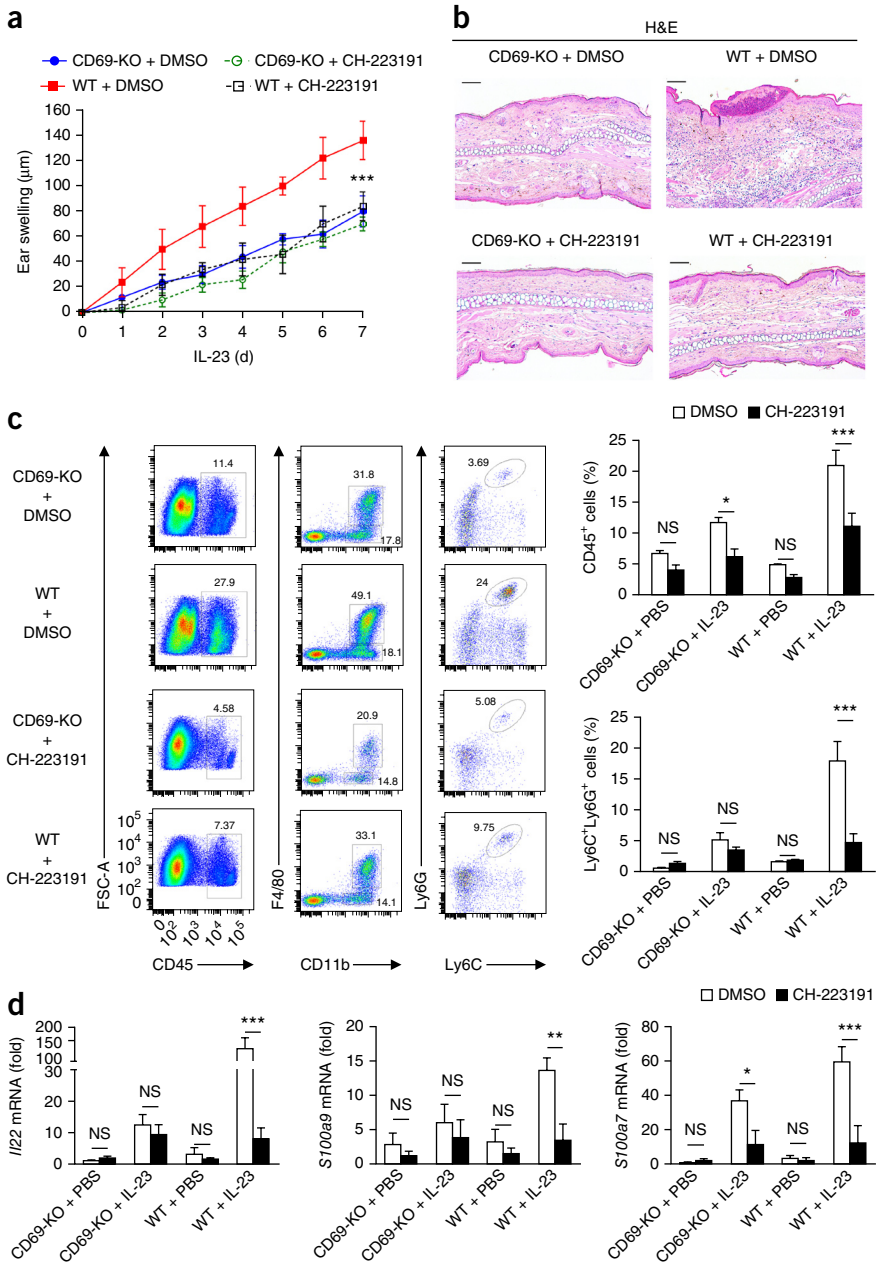

Figure 5 IL-23-induced skin inflammation is prevented by inhibition of AhR. (**a**) Ear thickness of CD69-deficient and wild-type mice during the administration of seven doses of IL-23 (horizontal axis) with concomitant daily intraperitoneal injection of CH-223191 or vehicle (DMSO). (**b**) H&E-stained sections of ears from wild-type and CD69-deficient mice treated intradermally with seven doses of IL-23 along with systemic administration of CH-223191 or DMSO. Scale bars, 100 μm; original magnification, ×10. (**c**) Flow cytometry of cells from wild-type and CD69-deficient mice treated as in **a** (left margin). Numbers adjacent to outlined areas indicate percent $CD45^+$ cells among live gated cells (left), $CD11b^+F4/80^+$ macrophages (top) or $CD11b^+F4/80^-$ cells (bottom) among $CD45^+CD11c^-$ live gated cells (middle), or $Ly6G^+Ly6C^+$ neutrophils among $CD11b^+F4/80^-$ gated cells (right). Right, frequency of $CD45^+$ cells among live-gated skin cells (top) and of $Ly6C^+Ly6G^+$ cells in the $CD45^+CD11c^-CD11b^+F4/80^-$ subset (bottom) in wild-type and CD69-deficient mice treated with PBS or IL-23 (horizontal axis) and with CH-223191 or DMSO (key). (**d**) Quantitative PCR analysis of *Il22*, *S100a9* and *S100a7* mRNA in the skin of mice as in **a** (presented as in **Fig. 2a**,**b**). $*P < 0.05$, $**P < 0.01$ and $***P < 0.001$ (two-way ANOVA with Bonferroni's multiple-comparisons test). Data are representative of two independent experiments with similar results (mean ± s.d. (**a**) or mean + s.e.m. (**c**,**d**); $n = 5$ mice per group).

similar ear swelling and expression of *Il1b*, *S100a8* and *S100a9* in CD69-deficient skin and wild-type skin (**Supplementary Fig. 3a**). These observations suggested that the effect of IL-22 in the context of IL-23-induced skin inflammation was independent of CD69 expression.

Direct involvement of AhR in the secretion of IL-22 by dermal γδ T cells was addressed by simultaneous administration of three intradermal injections of IL-23 into the ears of AhR-deficient and wild-type mice, as well as intraperitoneal administration of brefeldin A. Flow cytometry of skin-cell suspensions showed fewer $IL\text{-}22^+$ dermal γδ T cells in AhR-deficient mice than in wild-type mice, while the number of $IL\text{-}17^+$ γδ T cells was increased similarly in the skin of each genotype (**Supplementary Fig. 3b**). In addition, we stimulated sorted CD69-deficient and wild-type dermal γδ T cells *in vitro* with IL-23 plus IL-1β in the presence of the AhR inhibitor CH-223191, which prevented secretion of IL-22 by cells of each genotype (**Supplementary Fig. 3c**). To assess whether IL-22 secretion depended on CD69 in γδ T subsets in locations other than the skin, we studied splenic $CD27^-$ γδ T cells, which secrete IL-17 and IL-22 after being stimulated with IL-23 (ref. 31). These cells expressed CD69 after being stimulated with IL-23 and/or IL-1β (**Supplementary Fig. 3d**). Splenic $CD27^-$ γδ T cells from CD69-deficient mice had lower expression of IL-22 than that of their wild-type counterparts, and this was abrogated by CH-223191 (**Supplementary Fig. 3e**). These observations indicated that activation of AhR was required for CD69 to regulate the IL-23-induced IL-22 expression.

To address whether inhibition of AhR controlled IL-23-dependent skin inflammation, we injected IL-23 intradermally into wild-type and CD69-deficient mice, together with daily intraperitoneal administration of CH-223191. This treatment decreased inflammation in wild-type mice but had a very modest effect on CD69-deficient mice (**Fig. 5a**,**b**). Systemic administration of CH-223191 also reduced the number of IL-23-driven $Ly6G^+Ly6C^+$ neutrophils in wild-type skin to numbers similar to those in CD69-deficient skin (**Fig. 5c**). Also, the expression of *Il22* mRNA and of the IL-22 target genes *S100a9* and *S100a7* in whole skin was significantly lower in wild-type mice that received CH-223191 plus IL-23 than in wild-type mice that received IL-23 alone and was similar to that in CD69-deficient mice treated with IL-23 (**Fig. 5d**). These results indicated that AhR and IL-22 contributed to skin inflammation controlled by CD69.

CD69 associates with LAT1-CD98 and controls amino acid uptake

To address the mechanism by which CD69 regulated the AhR-mediated expression of IL-22, we used mass spectrometry to explore possible interactions of CD69 with regulators of AhR. We found that CD69 associated with several nutrient transporters, including CD98, LAT1, MOT1 and GTR1 (**Supplementary Table 1** and **Supplementary Fig. 4a**). The LAT1-CD98 complex is a major intake receptor for aromatic amino acids such as L-Trp, which is a source of ligands for AHR[14]. Immunoprecipitation experiments showed that CD69 associated with both chains of the LAT1-CD98 transporter in human Jurkat T cells activated with PMA and ionomycin (**Fig. 6a**). Confocal imaging and a proximity-ligation assay also indicated an

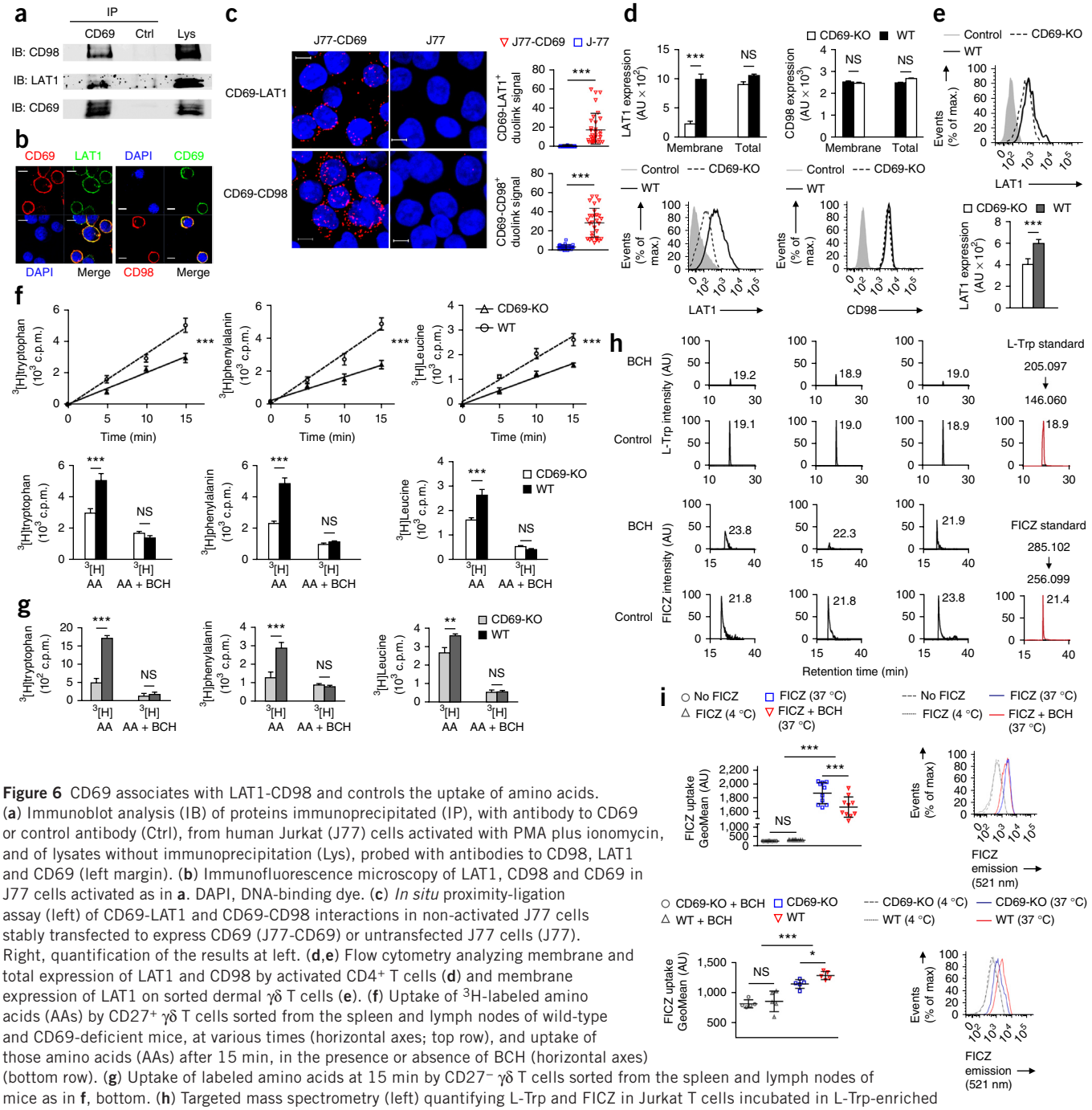

Figure 6 CD69 associates with LAT1-CD98 and controls the uptake of amino acids. (**a**) Immunoblot analysis (IB) of proteins immunoprecipitated (IP), with antibody to CD69 or control antibody (Ctrl), from human Jurkat (J77) cells activated with PMA plus ionomycin, and of lysates without immunoprecipitation (Lys), probed with antibodies to CD98, LAT1 and CD69 (left margin). (**b**) Immunofluorescence microscopy of LAT1, CD98 and CD69 in J77 cells activated as in **a**. DAPI, DNA-binding dye. (**c**) *In situ* proximity-ligation assay (left) of CD69-LAT1 and CD69-CD98 interactions in non-activated J77 cells stably transfected to express CD69 (J77-CD69) or untransfected J77 cells (J77). Right, quantification of the results at left. (**d**,**e**) Flow cytometry analyzing membrane and total expression of LAT1 and CD98 by activated CD4$^+$ T cells (**d**) and membrane expression of LAT1 on sorted dermal γδ T cells (**e**). (**f**) Uptake of ^{3}H-labeled amino acids (AAs) by CD27$^+$ γδ T cells sorted from the spleen and lymph nodes of wild-type and CD69-deficient mice, at various times (horizontal axes; top row), and uptake of those amino acids (AAs) after 15 min, in the presence or absence of BCH (horizontal axes) (bottom row). (**g**) Uptake of labeled amino acids at 15 min by CD27$^-$ γδ T cells sorted from the spleen and lymph nodes of mice as in **f**, bottom. (**h**) Targeted mass spectrometry (left) quantifying L-Trp and FICZ in Jurkat T cells incubated in L-Trp-enriched medium and left untreated (Control) or treated with BCH, presented as mass-spectrometry-2-extracted values reflecting the intensity (AU) of each compound in each sample, with retention times used for identification (three biological replicates: top, middle, left); far right (red), ion chromatograms of reference standards for L-Trp and FICZ (confirmation of retention times; presented as at left). (**i**) Flow cytometry analyzing the uptake of FICZ by wild-type activated CD4$^+$ T cells after 16 h of incubation with no FICZ or 1 μM FICZ (top row) or by CD69-deficient and wild-type activated CD4$^+$ T cells after 1 h of incubation with 100 nM FICZ (bottom row), with or without BCH, at 4 °C or 37 °C (key). Each symbol (**c**,**i**) represents an individual replicate (cell (**c**) or well (**i**)); small horizontal lines indicate the mean (± s.d.). $^*P < 0.05$, $^{**}P < 0.01$ and $^{***}P < 0.001$ (unpaired *t*-test (**c**,**e**) or one- or two-way ANOVA and Newman-Keuls or Bonferroni's test (**d**,**f**,**g**)). Data are representative of two experiments (**a**–**c**,**f**,**g**,**i**; mean + s.e.m. in **f**,**g**), three experiments with at least $n = 5$ replicates (wells) per group (**d**,**e**; mean + s.d.) or three independent experiments with one biological replicate (**h**).

association of CD69 with CD98 and LAT1 on the plasma membrane of activated Jurkat T cells (**Fig. 6b**,**c**).

Activated $CD4^+$ T cells from CD69-deficient mice had lower surface expression of LAT1 but not lower total expression of LAT1 than that of their wild-type counterparts, while plasma-membrane expression and global expression of CD98 were similar in cells of each genotype (**Fig. 6d**). Membrane expression of LAT1 was also significantly higher in sorted wild-type dermal γδ T cells than in their CD69-deficient counterparts (**Fig. 6e**). After stimulation with antibody to the invariant signaling protein CD3 (anti-CD3), wild-type $CD4^+$ T cells and CD69-deficient $CD4^+$ T cells showed a similar increase in *Slc7a5* mRNA (which encodes LAT1) and *Slc3a2* mRNA (which encodes CD98) (**Supplementary Fig. 4b**); this suggested that CD69 might have been regulating LAT1 dynamics and/or its stability at the membrane. Moreover, no significant difference between activated $CD4^+$ T cells from CD69-deficient and those from wild-type mice was observed in the expression of mRNA encoding other amino acid transporters, except for higher expression of *Slc38a2* mRNA (which encodes the transporter SNAT2), regulated by amino-acid starvation[32], in CD69-deficient $CD4^+$ T cells than in their wild-type counterparts (**Supplementary Fig. 4c**).

Assays of the uptake of ^{3}H-labeled L-Trp, L-Phe and L-Leu showed that CD69-deficient γδ T cells isolated from spleen and lymph nodes had slower uptake of L-Trp via LAT1 than that of their wild-type counterparts (**Fig. 6f**,**g**). Likewise, less uptake of amino acids via LAT1 was detected in CD69-deficient $CD4^+$ T cells than in wild-type $CD4^+$ T cells (**Supplementary Fig. 5a**). Incubation with an antibody that promotes CD69 internalization[23] also triggered the internalization of LAT1 in $CD4^+$ T cells but had no effect on surface expression of CD98 (**Supplementary Fig. 5b**). HEK-293 human embryonic kidney cells were co-transfected with plasmids encoding CD69-GFP and LAT1-Cherry fusion proteins and then incubated with labeled anti-CD69; this showed co-internalization of CD69 and LAT1 (**Supplementary Fig. 5c**). Moreover, antibody-induced internalization of CD69 impaired the uptake of L-Trp and L-Phe in $CD4^+$ wild-type T cells relative to their uptake after treatment with control antibody, but it had no effect on amino acid uptake in CD69-deficient cells (**Supplementary Fig. 5d**). These observations indicated that CD69 was associated with LAT1 and regulated its localization at the plasma membrane and amino acid transport.

Mass-spectrometry analysis showed less intracellular accumulation of FICZ (a metabolic and photoxidative product of L-Trp that activates AhR) in Jurkat T cells cultured in L-Trp-enriched medium treated with the LAT1 inhibitor BCH than in cells not treated with BCH (**Fig. 6h**). Moreover, through use of the intrinsic fluorescence of FICZ, we observed enhanced intracellular transport of FICZ into T cells at 37 °C but not at 4 °C (**Fig. 6i**). Uptake of FICZ from the extracellular medium was lower in CD69-deficient T cells than in wild-type T cells, and these differences were abrogated by the LAT1 inhibitor (**Fig. 6i**). These results demonstrated that LAT1-CD98 facilitated the intracellular transport of FICZ in a CD69-regulated manner.

CD69-LAT1-CD98 regulate mTORC and AhR-mediated IL-22 expression

The LAT1-mediated transport of amino acids is required for activation of the metabolic-checkpoint-kinase complex mTORC pathway[33]. CD69-deficient and wild-type naive $CD4^+$ T cells were polarized toward T_H17 cells *in vitro* and mTORC signaling was assessed as phosphorylation of the kinases mTORC1, S6 and 4E-BP1 (at 24–96 h). CD69 expression was dispensable for early activation of mTORC at 24 h after engagement of the T cell antigen receptor (TCR) (**Supplementary Fig. 6a**). However, the maintenance of mTORC signaling is influenced by amino acid uptake[33]. T_H17 cells from CD69-deficient mice showed impaired phosphorylation of S6 and 4E-BP1 after 96 h relative to that of their wild-type counterparts (**Supplementary Fig. 6b**).

We next addressed the role of LAT1-CD98–mediated transport of aromatic amino acids in AhR-dependent responses. Addition of the LAT1 inhibitor BCH abrogated IL-22 production in CD69-deficient and wild-type T_H17 cells (**Supplementary Fig. 6c**). In contrast, addition of the AhR ligand FICZ induced the secretion of IL-22 from cells of each genotype (**Supplementary Fig. 6c**). Culture of T_H17 cells with L-Trp-enriched Iscove's modified Dulbecco's medium (IMDM)[13] restored the secretion of IL-22 from CD69–deficient T_H17 to the secretion of IL-22 by wild-type cells (**Supplementary Fig. 6c**). Moreover, in the presence of LAT1 inhibitor BCH, the IL-22 expression in dermal γδ T cells stimulated *in vitro* with IL-23 plus IL-1β was reduced in wild-type cells to an amount similar to that observed in their CD69-deficient counterparts (**Fig. 7a**). Conversely, culture in IMDM or the addition of FICZ induced similar IL-22 expression in CD69-deficient dermal γδ T cells and wild-type dermal γδ T cells (**Fig. 7a**). Supplementation of RPMI medium with L-Trp also increased the release of IL-22 from CD69-deficient and wild-type $CD4^+$ T_H17 cells (**Fig. 7b**), although differences in IL-17 secretion remained (**Fig. 7b**). Expression of the AhR-regulated genes *Ahrr* and *Il22* was higher in CD69-deficient and wild-type $CD4^+$ naive cells polarized *in vitro* into the T_H17 subset and cultured in RPMI medium supplemented with L-Trp or IMDM than in cells activated with anti-CD3 and antibody to the costimulatory receptor CD28 (anti-CD28) (the 'T_H0-polarizing' condition) (**Fig. 7c**). The addition of BCH decreased the expression of *Ahrr* and *Il22* mRNA in CD69-deficient and wild-type cells (**Fig. 7c**).

Psoriatic skin displays increased expression of the tryptophan-degrading enzymes IDO (indoleamine 2,3-dyoxigenase) and TDO (tryptophan 2,3-dioxygenase), which catalyze the first step in L-Trp catabolism by the kynurenine pathway, and higher expression of the enzyme L-kynureninase, which further degrades kynurenine[34]. Thus, we assessed their expression in whole skin after intradermal injection of IL-23 alone or IL-23 plus IL-22. The expression of mRNA encoding IDO or L-kynureninase was induced similarly in CD69-deficient skin and wild-type skin, while the expression of mRNA encoding TDO was not induced by IL-23 (**Supplementary Fig. 6d**).

To determine whether uptake of L-Trp *in vivo* by dermal γδ T cells modulated psoriasis in CD69-deficient and wild-type mice, we administered L-Trp daily (intraperitoneally) simultaneously with intradermal injection of IL-23. The administration of L-Trp resulted in similar skin swelling in CD69-deficient mice and wild-type mice (**Fig. 7d**) and similar numbers of infiltrating $CD45^+CD11b^+F4/80^+$ macrophages and $CD45^+CD11b^+F4/80^-Ly6G^+Ly6C^+$ neutrophils in the skin of CD69-deficient mice and that of wild-type mice (**Fig. 7e**,**f**). We also observed similar numbers of IL-22^+ dermal γδ T cells in CD69-deficient mice and wild-type mice following the administration of L-Trp (**Fig. 7g**). Hence, these results indicated that CD69 regulated the surface expression of LAT1, the uptake of L-Trp, an intracellular increase in FICZ, and subsequent AhR activation and IL-22 secretion in dermal γδ T cells (**Supplementary Fig. 7**).

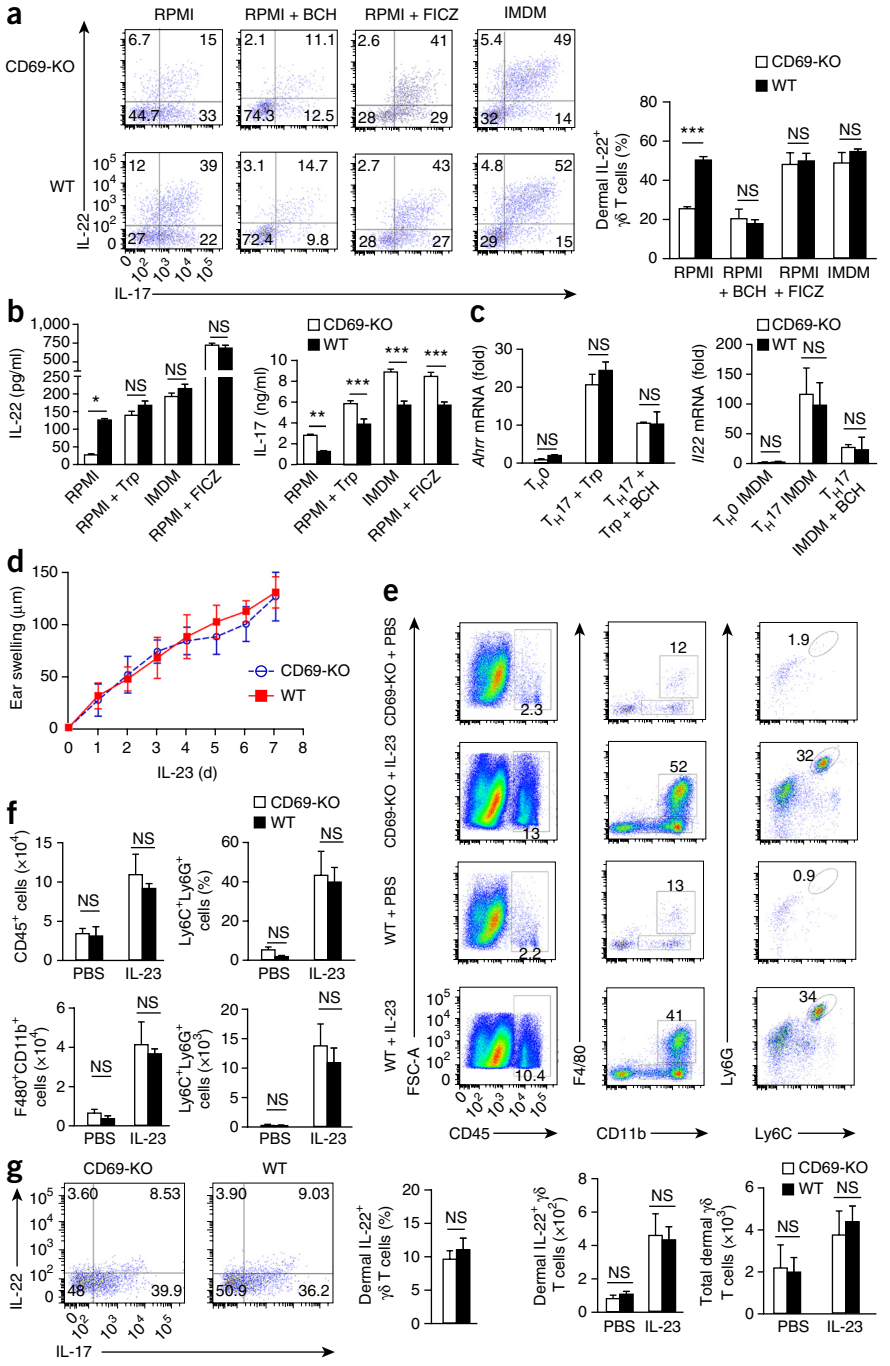

Figure 7 CD69 regulates AhR-induced secretion of IL-22 by dermal γδ T cells *in vitro* and *in vivo* through control of L-Trp uptake. (**a**) Flow cytometry (left) analyzing the expression of IL-22 and IL-17 by wild-type and CD69-deficient sorted dermal γδ T cells stimulated *in vitro* with IL-23 plus IL-1β in RPMI medium alone or supplemented with BCH or FICZ, or in IMDM (above plots). Right, frequency of IL-22$^+$ cells as at left. (**b**) ELISA of IL-22 and IL-17 in supernatants of wild-type and CD69-deficient CD4$^+$ T_H17 cells cultured in RPMI medium alone or supplemented with L-Trp or FICZ, or in IMDM (horizontal axes). (**c**) Quantitative PCR analysis of *Ahrr* and *Il22* mRNA in T_H0 and T_H17 cells cultured for 48 h *in vitro* in various conditions in RPMI medium (for *Ahrr*) or in IMDM (for *Il22*) (horizontal axes) (presented as in **Fig. 2a**,**b**). (**d**) Ear swelling of CD69-deficient and wild-type mice during the administration of IL-23 plus L-Trp. (**e**) Flow cytometry of cells in ears from mice given systemic injection of L-Trp in addition to intradermal administration of PBS or IL-23 (numbers adjacent to outlined areas, as in **Fig. 5c**). (**f**) Frequency (top right) and total number (top left and bottom row) of CD45$^+$ cells from live gated skin cells (top left) and of Ly6C$^+$Ly6G$^+$ cells in the CD45$^+$CD11b$^+$F4/80$^-$ subset (top right). (**g**) Flow cytometry (left) of dermal γδ T cells in CD69-deficient and wild-type mice treated with IL-23 and L-Trp and given injection of brefeldin A. Right, frequency and total number of IL-22$^+$ cells, and total dermal γδ T cells. Each symbol (**c**,**i**) represents an individual replicate (well); small horizontal lines indicate the mean (± s.d.). $*P < 0.05$, $**P < 0.01$ and $***P < 0.001$ (two-way ANOVA and Bonferroni's test). Data are representative of two experiments (mean + s.e.m. (**a**–**c**,**f**,**g**) or mean ± s.d. (**d**); $n = 5$ mice per group in **d**–**g**).

Upregulation of CD69, LAT1 and IL-22 in psoriasis

We next assessed whether CD69$^+$ γδ T cells were present in skin samples from patients with moderate to severe psoriasis. CD69 expression was detected by immunofluorescence in $V_\gamma9^+$ T cells in psoriatic skin lesions (**Fig. 8a**). The frequency of $V_\gamma9^+$CD69$^+$ T cells positively correlated with the psoriasis area severity index (**Fig. 8b**). Immunofluorescence staining showed that IL-22-secreting $V_\gamma9^+$ T cells in the dermal layer expressed CD69 (**Fig. 8c**). In agreement with that, expression of *IL22* and *TNF* mRNA was higher in psoriatic skin than in biopsies of healthy skin (**Fig. 8d**).

The frequency of circulating CD69$^+$CLA$^+$$V_\gamma9^+$ T cells was greater in psoriatic patients than in healthy control subjects (**Fig. 8e**). To assess the ability of these cells to produce IL-22, we stimulated circulating γδ T cells from psoriatic patients *in vitro* with a cytokine 'cocktail' (IL-23 plus IL-1β plus IL-6 plus TGF-β). IL-22 expression in human $V_\gamma9^+$ γδ T cells was decreased by the addition of inhibitors of AhR or LAT1 (**Fig. 8f**,**g**). Quantitative RT-PCR analysis of mRNA from whole-skin biopsies showed significantly higher expression of *SLC7A5* and *CD69* mRNA in psoriatic lesions than in unaffected regions, whereas *SLC3A2* mRNA was not expressed differentially in these regions (**Fig. 8h**). These results demonstrated LAT1-mediated regulation of AhR and IL-22 in γδ T cells from patients with psoriasis.

DISCUSSION

The pathogenesis of psoriasis involves cross-talk between skin-resident innate immune cells and keratinocytes, which is orchestrated by cytokines such as IL-22 and IL-17 (refs. 1,35). Here we found that CD69 associated with the transporter complex LAT1-CD98 and enhanced the uptake of L-Trp, a metabolic precursor of AhR ligands that promoted IL-22 secretion[13,14]. The transcriptional activity of STAT3 induced by IL-22 in keratinocytes upregulates the expression of pro-inflammatory molecules such as keratin 17, S100A7, S100A8 and S100A9, as well as several CXCL chemokines[6,36].

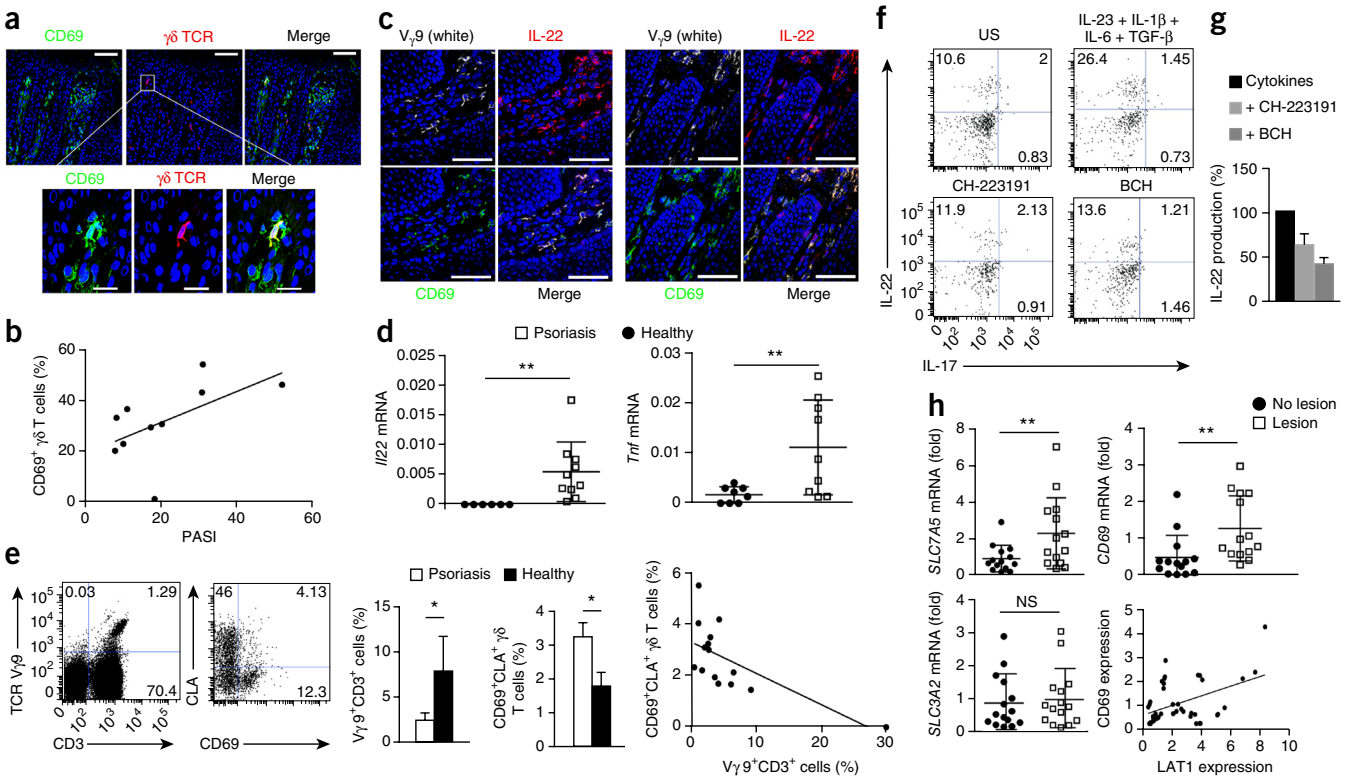

Figure 8 CD69 expression is detected in skin and circulating $V_\gamma9^+$ T cells from psoriatic patients. (**a**) Microscopy of frozen section of human psoriatic lesions immunostained for CD69, the γδ TCR and nuclei (DAPI); outlined area (top middle) is enlarged below. Scale bars, 50 μm (top row) or 25 μm (bottom row). (**b**) Correlation between the frequency of dermal $V_\gamma9^+CD69^+$ T cells and the clinical psoriasis area severity index (PASI) of psoriatic patients ($r = 0.64$ (Spearman test); $P < 0.05$. (**c**) Microscopy of frozen sections from psoriatic lesions immunostained for $V_\gamma9$, IL-22 and CD69. Scale bars, 50 μm. (**d**) Quantitative PCR analysis of *IL22* and *TNF* mRNA in lesional skin from patients and skin from healthy subjects; results (calculated by the standard-curve method) were normalized to those of the control gene *ACTB*. (**e**) Flow cytometry analyzing the expression of $V_\gamma9$ and CD3 (left) and of CLA and CD69 by $CD3^+V_\gamma9^+$ gated cells (right) among peripheral blood mononuclear cells from a psoriatic patient. Middle, frequency of $V_\gamma9^+CD3^+$ cells (left) among live cells and of CLA^+ and $CD69^+$ cells among $V_\gamma9^+$ peripheral γδ T cells from psoriatic patients and healthy subjects. Far right, frequency of $CD69^+CLA^+V_\gamma9^+$ cells plotted against that of $V_\gamma9^+CD3^+$ cells. (**f**) Flow cytometry analyzing the expression of IL-22 and IL-17 by peripheral γδ T cells obtained from psoriatic patients, then subjected to population expansion and left unstimulated (US) or stimulated with various cytokines alone (top left) or in the presence of CH-223191 (bottom left) or BCH (bottom right). (**g**) ELISA of IL-22-producing cells as in **f**. (**h**) Quantitative PCR analysis of *SLC7A5*, *CD69* and *SLC3A2* in lesion and non-lesional areas of psoriatic patients (presented as in **Fig. 2a**,**b**), and correlation analysis of *CD69* and *SLC7A5* (bottom right: $r = 0.34$; $P = 0.02$). Each symbol (**b**,**d**,**e**,**h**) represents an individual donor; small horizontal lines indicate the mean (± s.d.). $^*P < 0.05$ and $^{**}P < 0.001$ (unpaired *t*-test). Data are representative of experiments with ten patients (**a**–**c**) ten patients and nine healthy subjects (**d**), nine patients and six healthy subjects (**e**; mean + s.e.m.), three patients (**f**), three patients and six healthy subjects (pooled) (**g**; mean + s.e.m.) or fifteen patients (**h**).

IL-22 also induces keratinocyte proliferation through the PI3K-Akt-mTORC signaling pathway[37]. The deficient expression of IL-22 and activation of STAT3 in the skin of CD69-deficient mice we found here provides a mechanistic link that explains the attenuated dermal inflammation and keratinocyte proliferation observed after administration of IL-23.

γδ TCR–deficient mice display attenuated psoriatic plaque formation in response to IL-23 (ref. 16) and imiquimod[18]. The role of CD69 as an enhancer of AhR activity and IL-22 release in γδ T cells *in vitro* and *in vivo* correlates well with clinical data showing increased CD69 expression on $V_\gamma9^+$ T cells from the skin and the bloodstream of psoriatic patients.

CD69 associated with the amino-acid transporter complex LAT1-CD98 on the plasma membrane of activated T cells and controlled the activation of mTORC. Further studies are needed to ascertain whether CD69 regulates other targets of mTORC, such as the autophagy route[38] and HIF-1α through AhR[39]. Different regions of CD98 control the uptake of amino acids and β_1-integrin-mediated cell proliferation[40]. However, published studies have shown no difference in the proliferation rate of CD69-deficient T lymphocytes and that of wild-type T lymphocytes[41], which suggests that the association of CD69 with the LAT1-CD98 complex in activated immune cells modulates the uptake of amino acids specifically.

Cytoplasmic L-Trp acts as a chromophore that is converted by exposure to light into active AhR ligands, including FICZ[13]. The characterization of a light-independent metabolic route for the generation of FICZ from the intracellular pool of L-Trp[14] suggests that regulation of entry of the precursor might determine the amount of cellular FICZ and AhR activation. Our results demonstrated that LAT1-CD98 regulated the intracellular accumulation of FICZ.

Inhibition of AhR protects against inflammation induced by IL-23 without substantial alteration of the keratinocyte layers. However, depletion of AhR in keratinocytes disrupts epidermal homeostasis, which enhances psoriasis in response to imiquimod, although lower expression of IL-22 in the skin of fully AhR-deficient mice than in the skin of wild-type mice has been detected[42]. Differences between the IL-23-induced psoriasis model and imiquimod-induced psoriasis model exist[2]. Toll-like-receptor-7-independent epidermal hyperproliferative responses induced by keratinocyte damage are involved in the induction of psoriasis in the imiquimod model[18,43].

AhR controls the terminal differentiation of epidermal cells and the expression of genes encoding proteins linked to skin barrier function, such as filaggrin[44,45]. Hence, AhR in keratinocytes is required for skin homeostasis, but its activation in inflammatory cells mediates inflammation.

CD69 did not affect the secretion of IL-17 by innate γδ T cells, in contrast to its effect on $CD4^+$ T_H17 T cells[27]. The greater secretion of IL-17 by CD69-deficient $CD4^+$ T_H17 cells than by wild-type $CD4^+$ T_H17 cells is due to increased phosphorylation of STAT3 and increased RORγt expression[27]. This was not observed in dermal γδ T cells, owing to the fact that the transcription factors that control the T_H17 differentiation $CD4^+$ T cells, such as STAT3, are not required for the development of IL-17^+ (RORγt$^+$) γδ T cells that originated in fetal thymus[46,47].

Prevention of the uptake of L-Trp via LAT1 abrogated the AhR-dependent secretion of IL-22 from human peripheral γδ T cells from psoriatic patients, which would suggest a possible role for the uptake of dietary L-Trp in psoriasis. Notably, *in vivo* administration of L-Trp increased the severity of inflammatory responses elicited by IL-23 independently of CD69 expression. Overall, these data indicate that L-Trp catabolism has an important role in the pathophysiology of psoriasis, not only due to the regulation of kynurenine but also by its effect on other metabolites that might contribute to skin inflammation. In conclusion, our study has established a biological role for CD69 in the control of amino acid uptake and the regulation of AhR activation and IL-22 expression in γδ and T_H17 cells and indicates that CD69 contributes to the development of psoriasis.

METHODS

Methods and any associated references are available in the online version of the paper.

Note: Any Supplementary Information and Source Data files are available in the online version of the paper.

ACKNOWLEDGMENTS

We thank D. Rotin (University of Toronto) for the plasmid for the expression of LAT1-mCherry; P. Taylor (University of Dundee) for antiserum to human LAT1; M. Navarro (Universidad Autónoma de Madrid, Spain) for IL-23R-GFP reporter mice; S. Bartlett for English editing; and T. Hernandez and R. Brid Doohan for technical assistance with immunohistochemistry. Supported by the Spanish Ministry of Economy and Competitiveness (SAF2011-25834 and SAF2014-55579-R to F.S.-M.; SAF2011-27330 to P.M.; and SAF2013-42850 to M.F.), Comunidad de Madrid (INDISNET-S2011/BMD-2332 to F.S.-M.; and 2010/BMD-2332 from M.F. and F.S.-M.), Instituto Salud Carlos III (Red Cardiovascular RD 12-0042-0056 to F.S.-M.; BIOIMID to M.F. and F.S.-M.), the European Research Council (ERC-2011-AdG 294340-GENTRIS to F.S.-M.) and the Ramón Areces foundation (M.F. and F.S.-M.).

AUTHOR CONTRIBUTIONS

D.C. performed mice experimentation, analyzed and interpreted data and wrote the manuscript; M.L.S. collaborated on mice experimentation, data interpretation and writing of the manuscript; H.d.l.F. performed analysis of psoriatic patients; R.S.-D. and O.M.-G. performed quantitative PCR; I.J., A.F. and J.V. performed proteomic and metabolic-mass spectrometry analyses; C.P. contributed expertise in radioactive assays; M.F., M.V.-M. and P.M.F.-S. provided reagents and helped with the revision of the manuscript; E.D. provided biopsies from psoriatic patients and their clinical diagnostics; P.M. helped to design research, provided reagents, collaborated in data interpretation and manuscript writing; and F.S.-M. planned research, discussed results and collaborated in writing the manuscript.

COMPETING FINANCIAL INTERESTS

The authors declare no competing financial interests.

1. Di Meglio, P., Villanova, F. & Nestle, F.O. Psoriasis. *Cold Spring Harb. Perspect. Med.* **4**, a015354 (2014).
2. Lowes, M.A., Suárez-Fariñas, M. & Krueger, J.G. Immunology of psoriasis. *Annu. Rev. Immunol.* **32**, 227–255 (2014).
3. Leonardi, C. *et al.* Anti-interleukin-17 monoclonal antibody ixekizumab in chronic plaque psoriasis. *N. Engl. J. Med.* **366**, 1190–1199 (2012).
4. Chan, J.R. *et al.* IL-23 stimulates epidermal hyperplasia via TNF and IL-20R2-dependent mechanisms with implications for psoriasis pathogenesis. *J. Exp. Med.* **203**, 2577–2587 (2006).
5. Zheng, Y. *et al.* Interleukin-22, a T_H17 cytokine, mediates IL-23-induced dermal inflammation and acanthosis. *Nature* **445**, 648–651 (2007).
6. Wolk, K. *et al.* IL-22 and IL-20 are key mediators of the epidermal alterations in psoriasis while IL-17 and IFN-γ are not. *J. Mol. Med.* **87**, 523–536 (2009).
7. Van Belle, A.B. *et al.* IL-22 is required for imiquimod-induced psoriasiform skin inflammation in mice. *J. Immunol.* **188**, 462–469 (2012).
8. Prans, E. *et al.* Copy number variations in *IL22* gene are associated with psoriasis vulgaris. *Hum. Immunol.* **74**, 792–795 (2013).
9. Shimauchi, T. *et al.* Serum interleukin-22 and vascular endothelial growth factor serve as sensitive biomarkers but not as predictors of therapeutic response to biologics in patients with psoriasis. *J. Dermatol.* **40**, 805–812 (2013).
10. Wolk, K. *et al.* IL-22 regulates the expression of genes responsible for antimicrobial defense, cellular differentiation, and mobility in keratinocytes: a potential role in psoriasis. *Eur. J. Immunol.* **36**, 1309–1323 (2006).
11. Martin, B., Hirota, K., Cua, D.J., Stockinger, B. & Veldhoen, M. Interleukin-17-producing γδ T cells selectively expand in response to pathogen products and environmental signals. *Immunity* **31**, 321–330 (2009).
12. Qiu, J. *et al.* The aryl hydrocarbon receptor regulates gut immunity through modulation of innate lymphoid cells. *Immunity* **36**, 92–104 (2012).
13. Veldhoen, M., Hirota, K., Christensen, J., O'Garra, A. & Stockinger, B. Natural agonists for aryl hydrocarbon receptor in culture medium are essential for optimal differentiation of Th17 T cells. *J. Exp. Med.* **206**, 43–49 (2009).
14. Smirnova, A. *et al.* Evidence for new light-independent pathways for generation of the endogenous aryl hydrocarbon receptor agonist FICZ. *Chem. Res. Toxicol.* **29**, 75–86 (2016).
15. Sinclair, L.V. *et al.* Control of amino-acid transport by antigen receptors coordinates the metabolic reprogramming essential for T cell differentiation. *Nat. Immunol.* **14**, 500–508 (2013).
16. Cai, Y. *et al.* Pivotal role of dermal IL-17-producing γδ T cells in skin inflammation. *Immunity* **35**, 596–610 (2011).
17. Laggner, U. *et al.* Identification of a novel proinflammatory human skin-homing Vγ9Vδ2 T cell subset with a potential role in psoriasis. *J. Immunol.* **187**, 2783–2793 (2011).
18. Pantelyushin, S. *et al.* Rorγt$^+$ innate lymphocytes and γδ T cells initiate psoriasiform plaque formation in mice. *J. Clin. Invest.* **122**, 2252–2256 (2012).
19. Ahlfors, H. *et al.* IL-22 fate reporter reveals origin and control of IL-22 production in homeostasis and infection. *J. Immunol.* **193**, 4602–4613 (2014).
20. Sumaria, N. *et al.* Cutaneous immunosurveillance by self-renewing dermal γδ T cells. *J. Exp. Med.* **208**, 505–518 (2011).
21. González-Amaro, R., Cortés, J.R., Sánchez-Madrid, F. & Martín, P. Is CD69 an effective brake to control inflammatory diseases? *Trends Mol. Med.* **19**, 625–632 (2013).
22. Sancho, D. *et al.* CD69 downregulates autoimmune reactivity through active transforming growth factor-β production in collagen-induced arthritis. *J. Clin. Invest.* **112**, 872–882 (2003).
23. Martín, P. *et al.* The leukocyte activation antigen CD69 limits allergic asthma and skin contact hypersensitivity. *J. Allergy Clin. Immunol.* **126**, 355–365, 365.e1–365.e3 (2010).
24. Cruz-Adalia, A. *et al.* CD69 limits the severity of cardiomyopathy after autoimmune myocarditis. *Circulation* **122**, 1396–1404 (2010).
25. Radulovic, K. *et al.* CD69 regulates type I IFN-induced tolerogenic signals to mucosal CD4 T cells that attenuate their colitogenic potential. *J. Immunol.* **188**, 2001–2013 (2012).
26. Rutz, S., Eidenschenk, C. & Ouyang, W. IL-22, not simply a Th17 cytokine. *Immunol. Rev.* **252**, 116–132 (2013).
27. Martín, P. *et al.* CD69 association with Jak3/Stat5 proteins regulates Th17 cell differentiation. *Mol. Cell. Biol.* **30**, 4877–4889 (2010).
28. Mackay, L.K. *et al.* The developmental pathway for $CD103^+CD8^+$ tissue-resident memory T cells of skin. *Nat. Immunol.* **14**, 1294–1301 (2013).
29. Awasthi, A. *et al.* Cutting edge: IL-23 receptor gfp reporter mice reveal distinct populations of IL-17-producing cells. *J. Immunol.* **182**, 5904–5908 (2009).
30. Shiow, L.R. *et al.* CD69 acts downstream of interferon-α/β to inhibit S1P1 and lymphocyte egress from lymphoid organs. *Nature* **440**, 540–544 (2006).
31. Ribot, J.C. *et al.* CD27 is a thymic determinant of the balance between interferon-γ- and interleukin 17-producing gammadelta T cell subsets. *Nat. Immunol.* **10**, 427–436 (2009).
32. Kashiwagi, H., Yamazaki, K., Takekuma, Y., Ganapathy, V. & Sugawara, M. Regulatory mechanisms of SNAT2, an amino acid transporter, in L6 rat skeletal muscle cells by insulin, osmotic shock and amino acid deprivation. *Amino Acids* **36**, 219–230 (2009).
33. Taylor, P.M. Role of amino acid transporters in amino acid sensing. *Am. J. Clin. Nutr.* **99**, S223–S230 (2014).
34. Harden, J.L. *et al.* The tryptophan metabolism enzyme L-kynureninase is a novel inflammatory factor in psoriasis and other inflammatory diseases. *J. Allergy Clin. Immunol.* **137**, 1830–1840 (2016).

35. Rizzo, H.L. *et al.* IL-23-mediated psoriasis-like epidermal hyperplasia is dependent on IL-17A. *J. Immunol.* **186**, 1495–1502 (2011).
36. Boniface, K. *et al.* IL-22 inhibits epidermal differentiation and induces proinflammatory gene expression and migration of human keratinocytes. *J. Immunol.* **174**, 3695–3702 (2005).
37. Mitra, A., Raychaudhuri, S.K. & Raychaudhuri, S.P. IL-22 induced cell proliferation is regulated by PI3K/Akt/mTOR signaling cascade. *Cytokine* **60**, 38–42 (2012).
38. Finlay, D.K. *et al.* PDK1 regulation of mTOR and hypoxia-inducible factor 1 integrate metabolism and migration of $CD8^+$ T cells. *J. Exp. Med.* **209**, 2441–2453 (2012).
39. Mascanfroni, I.D. *et al.* Metabolic control of type 1 regulatory T cell differentiation by AHR and HIF1-α. *Nat. Med.* **21**, 638–646 (2015).
40. Fenczik, C.A. *et al.* Distinct domains of CD98hc regulate integrins and amino acid transport. *J. Biol. Chem.* **276**, 8746–8752 (2001).
41. Lauzurica, P. *et al.* Phenotypic and functional characteristics of hematopoietic cell lineages in CD69-deficient mice. *Blood* **95**, 2312–2320 (2000).
42. Di Meglio, P. *et al.* Activation of the aryl hydrocarbon receptor dampens the severity of inflammatory skin conditions. *Immunity* **40**, 989–1001 (2014).
43. Walter, A. *et al.* Aldara activates TLR7-independent immune defence. *Nat. Commun.* **4**, 1560 (2013).
44. van den Bogaard, E.H. *et al.* Genetic and pharmacological analysis identifies a physiological role for the AHR in epidermal differentiation. *J. Invest. Dermatol.* **135**, 1320–1328 (2015).
45. Furue, M. *et al.* Gene regulation of filaggrin and other skin barrier proteins via aryl hydrocarbon receptor. *J. Dermatol. Sci.* **80**, 83–88 (2015).
46. Serre, K. & Silva-Santos, B. Molecular mechanisms of differentiation of murine pro-inflammatory γδ T cell subsets. *Front. Immunol.* **4**, 431 (2013).
47. Shibata, K. *et al.* Notch-Hes1 pathway is required for the development of IL-17-producing γδ T cells. *Blood* **118**, 586–593 (2011).

ONLINE METHODS

Mice. Wild-type, CD69-deficient, OT-II and OT-II CD69-deficient mice (C57BL/6 background) were previously described[27]. Homozygous AhR-deficient and wild-type littermate mice (C57BL/6 background) were obtained from P. M. Fernández-Salguero's group (University of Extremadura, Badajoz, Spain). IL-23R-GFP.KI reporter mice (C57BL/6 background) were previously described[29]. For experiments with chimeric mice, wild-type B6SJL CD45.1 mice (Jackson) were used as donor of bone marrow progenitor cells. Sex- and age-matched mice (8–12 weeks) were used for *in vitro* and *in vivo* experiments. All animals were kept in pathogen-free conditions at the animal facility of Centro Nacional de Investigaciones Cardiovasculares. Experimental procedures were approved by the local Committee for Research Ethics and are in accordance to Spanish and European guidelines.

Human subjects. Patients with moderate to severe psoriasis that were recruited in the study had a psoriasis area and severity index of ≥8.0 and washout periods of 14 d for topical corticosteroids; 28 d for conventional systemic therapy, including corticosteroids, methotrexate, cyclosporine, acitretin and phototherapy; and 84 d for biological agents. Skin punch biopsies (5 mm) were obtained from lesional-plaque-type psoriasis and non-lesional area. Healthy skin biopsies were also collected from nine surgical patients without cutaneous disease. Half of each skin biopsy was immediately frozen and processed for RNA extraction, while remaining sample was embedded in OCT for immunofluorescence staining. Blood samples were also collected from ten psoriatic patients and five healthy volunteers, for flow cytometry analysis. The study was approved by the Hospital La Princesa ethics committee. All the participants gave their written informed consent.

Establishment of psoriasis-like model. CD69-deficient and wild-type mice were intradermally injected in the ears with 20 µl of vehicle (PBS) or 500 ng of recombinant mouse IL-23 (eBioscience) using a 33-gauge needle. Injections were repeated on alternate days for a total of seven to ten doses. Ear thickness was measured on days without injections with an AccuteRemote 0.5-mm-thickness gauge dial micrometer (TECLOCK). All measurements were performed blinded. Mice were sacrificed and skin samples were collected for staining with H&E and immunohistochemistry. If required, half of ears were rapidly frozen in liquid nitrogen for subsequent isolation of total RNA or detection of tissue cytokines. Recombinant mouse IL-22 (eBioscience) (500 ng in 20 µl of PBS) was intradermally injected alone or in combination with IL-23, where indicated. In addition, in some experiments mice received an intraperitoneal injection of CH-223191 (10 mg per kg body weight) or vehicle (DMSO) together with the IL-23 intradermal administration. When indicated, 250 µg/mice of secretion inhibitor brefeldin A dissolved in ethanol (SIGMA) was intraperitoneally administrated 5 h before sacrifice. For experiments with chimeric mice, wild-type and CD69-deficient mice (CD45.2 haplotype) were lethally irradiated (13 Gy divided in two sessions) and transplanted with 5×10^6 per mice of whole bone marrow cells obtained from B6 SJL (CD45.1 haplotype) wild-type mice. Reconstitution was allowed for 2 months before starting the protocol of IL-23 injections. In some experiments, mice received a daily intraperitoneal administration of L-Trp (50 mg per kg body weight) or its vehicle (DMSO) along the IL-23 protocol. L-Trp dose was chosen by published assays that proved it to be safe for mice and that it induced *Cyp1a1* transcriptional expression in the liver[48]. As described, FICZ can be found in light-oxidized preparation of L-Trp[13]; for this reason, fresh solutions were daily prepared and kept protected from light.

Skin histology and immunohistochemistry staining. Skin samples were fixed in formaldehyde and embedded in paraffin using routine methods. Slices (4–5 µm) were stained with H&E and analyzed by two evaluators 'blinded' to sample identity. Consecutive images were acquired at several magnifications with an optical microscope (DM2500; Leica) equipped with a CCD camera (DFC420; Leica), with Leica Application Suite software (version 4.3.0). Dermal and epidermal thickness were measured every 100 µm, from the ear surface to a depth of about 5 mm, using ImageJ software. For immunohistochemical staining, skin sections were deparaffinized, boiled in antigen retrieval solution (10 mM sodium citrate, 0,05% Tween 20, pH6), and incubated with the following primary monoclonal antibodies (**Supplementary Table 2**): rabbit anti-mouse Ki67 (Master Diagnostica),rat anti-mouse F4/80 and Ly6G (Abcam), rabbit anti-mouse STAT3, phospho-STAT3 (Tyr 705) and phospho-STAT3 (Ser727) (Cell Signaling); followed by specific secondary antibodies from Dako (**Supplementary Table 2**): envision flex system for Ki67, Rabbit anti rat HRP for F480 and Ly6G; and Goat anti Rabbit HRP for STAT3-related antibodies. Slides were developed with DAB substrate (Dako K3468) and then counterstained with Mayers hematoxylin. Epidermal $Ki67^+$ frequency was determined as the number of $Ki67^+$ nuclei observed each 100 µm, also from the ear surface to a depth of about 5 mm, $n = 5$ mice per group. STAT3 staining in keratinocytes was quantified in at least five fields (×40 magnification) from each IL-23-treated mouse (five mice per group). Fields were quantified for mean gray value in the epidermal layer with ImageJ software. Percentage of epidermal area stained for STAT3 was also assessed. Nuclear staining of each phosphorylation site for STAT3 in keratinocytes was also counted as indicative of its transcriptional activity.

RNA extraction and real-time quantitative PCR. RNA from mouse and human samples was isolated using a QIAGEN RNeasy Kit (Qiagen). Residual DNA contamination was removed with the Turbo DNA-free Kit (Ambion). Total RNA (200ng) was reverse transcribed to cDNA with a Reverse Trancription Kit (Applied Biosystem). Quantitative PCR was then performed in an AB7900_384 (Applied Biosystem) using SYBR Green (Applied Biosystems) as reporter. Gene-specific primers used are listed in **Supplementary Table 3**. Expression of each gene of interest was normalized to at least two housekeeping genes (*Actb* or *Gapdh*). Data (calculated by the $2^{-\Delta\Delta Ct}$ method or the standard-curve method (for human samples)) are presented as results for CD69-deficient mice relative to those of wild-type mice samples, or treated samples relative to control samples, or psoriatic patients relative to the mean value obtained for healthy donors.

Flow cytometry and sorting of skin γδ T cells. Animals were euthanized and ears were collected and digested with Liberase TM (Roche) (0.25 mg/ml in free-serum medium RPMI), for 60 min at 37 °C. Enzyme was inhibited by adding 50 ml of PBS supplemented with 0.5% of BSA and 0.05mM of EDTA (PBS-BSA-EDTA) and tissue was mechanically disrupted and filtered to obtain a skin cell suspension. Epidermis and dermis separation was conducted after incubation of ears with trypsin-EDTA solution 1X (Sigma), 45 min at 37 °C. The two layers were separated with forceps, and the epidermis was directly homogenized while the dermis was incubated with Liberase TM by 30 min. Incubation of skin cell suspensions with anti-FcRII/III (clone 2.4G2; **Supplementary Table 2**) was always conducted before staining. For flow cytometry analysis of IL-23 -induced inflammation the following anti-mouse antibodies were used (**Supplementary Table 2**): CD45, F480 and γδTCR obtained from eBioscience, CD11c, CD11b, GR1, Ly6G, Ly6C and CD3 from BD Bioscience. Absolute count of cells in the skin was conducted using BD Trucount Tubes (BD). For sorting skin γδ T cells, cell suspensions obtained from ears were stained with DAPI, anti-CD3 (BD Biosciences) and anti-γδTCR (eBioscience). Directed labeled antibodies against mouse IL-23R (R&D) and RORγt (EBioscience) (**Supplementary Table 2**) were also used in skin suspensions. To analyze the expression of CD69 in human circulating γδ T cells, freshly obtained peripheral blood mononuclear cells (PBMCs) (1×10^6) from psoriatic patients and healthy subjects were stained with the following mouse anti-human mAbs: anti-CLA (BD Bioscience), anti-TCR $V_\gamma 9$ (BioLegend) and anti-CD8, anti-CD69, anti-CD4 and anti-CD3 (BD Bioscience) (**Supplementary Table 2**). Cell samples were acquired in a FACSCanto Flow Cytometer (BD), and analyzed with FlowJo software (Tree Star).

Cell cultures for T_H17 and γδ T cells. Cells were routinely cultured in RPMI 1640 medium (Sigma-Aldrich) supplemented with 5% FCS, 2 mM L-glutamine, 100 U/ml penicillin 100 µg/ml streptomycin, and 50 nM of β-mercaptoethanol. In some cases, IMDM (Sigma-Aldrich) was used, supplemented as for RPMI. Also, in some cases, RPMI medium was supplemented with 11 mg/liter L-Trp (Invitrogen) to adjust it to the concentrations found in IMDM. Naive $CD4^+$ T cells were obtained by negative selection using an auto-MACSTM Pro Separator (Miltenyi Biotec) and subjected to *in vitro* T_H17 differentiation (1×10^6 cells/ml) with the following cytokine cocktail: blocking anti-IFN-γ (5 µg/ml) and anti-IL-4 (5 µg/ml) mAbs, IL-6 (50 ng/ml), IL-23 (10 ng/ml),

IL-1β (10 ng/ml) and TGF-β1 (5 ng/ml) for 2-4 d (**Supplementary Table 2**). Naive CD4$^+$ T cells obtained from OT-II and OT-II CD69-deficient were cultured in the presence of irradiated antigen-presenting cells (T cell–depleted splenocytes) and OVA peptide 323-339 (OVA; 10 μg/ml). Those experiments with OT-II mice were specifically used for flow cytometry analysis and ELISA. When T_H17 cells were required for mRNA analysis expression and western blot, naive CD4 T cells were isolated from wild-type and CD69-deficient mice and were activated with plate-bound anti-CD3 (5 μg/ml) plus anti-CD28 (2 μg/ml) (**Supplementary Table 2**), using the same cytokine cocktail described above for OT-II mice. The AhR ligand 6-formylindolo (3,2-b) carbazole (FICZ) (Enzo Life Science) (350 nM), the AhR specific inhibitor CH-223191 (Sigma) (3 μM) and the LAT1/CD98 inhibitor 2-amino-2-norbornanecarboxylic acid (BCH) (Sigma) (50 mM) were added at the start of some cultures. Before intracellular cytokine staining, cells were restimulated for 4 h with 50 ng/ml phorbol dibutyrate (PMA) and 500 ng/ml ionomycin in the presence of brefeldin A (1 μg/ml) (BD Biosciences).

Sorted dermal and epidermal γδ T cells (1×10^4 cells/ml) from CD69-deficient and wild-type mice were incubated for 24 h on plate-bound anti-CD3 (5 μg/ml), soluble anti-CD28 (2 μg/ml) (**Supplementary Table 2**) and IL-23 plus IL-1β (10 ng/ml each one). For γδ T cells, no re-stimulation was required, and only brefeldin A (1 μg/ml) was added for last 4 h of culture.

Both γδ and *in vitro*–skewed T_H17 cells were fixed and permeabilized with Fix & Perm solution (BD Biosciences) and stained with anti-IL-22 (eBioscience) and anti-CD69, anti-CD25 and anti-IL-17 (BD Pharmingen) (**Supplementary Table 2**). IL-22 and IL-17 production in the cultures supernatants was quantified with the IL-22/IL-17 Ready-Set-Go ELISA kits (eBioscience). In some experiments, AhR nuclear expression was analyzed by flow cytometry using the Foxp3/Transcription Factor Staining Buffer Set (eBioscience) and rabbit anti-mouse AhR (Enzo Life Science) followed by Alexa-647 conjugated Goat anti rabbit. CD98 expression was detected with an Alexa 647-conjugated rat anti-mouse antibody (BioLegend) while for LAT1 expression a rabbit anti mouse antibody (Santa Cruz Biotech) followed by an Alexa-647 conjugated goat anti rabbit was used (all antibodies, **Supplementary Table 2**). Directed labeled 647-mouse anti STAT5 (pY694) and PE-mouse anti-STAT3 (pY705) (BD Bioscience) was used with Fix&Perm kit (life technologies) modified for methanol permeabilization (antibodies, **Supplementary Table 2**). Mouse isotype-matched control antibodies obtained from BD were used as required (**Supplementary Table 2**).

IL-22 production in human γδ T cells. PBMCs from psoriatic patients ($n = 3$) were adjusted at 1×10^6 cells/ml in culture medium EX-VIVO 15 (Lonza, Belgium) supplemented with L-Trp (15 mg/L) and expanded with zoledronic acid (5 μM) as previously reported[49]. At day 0 (d0), PBMCs (1×10^6) were stimulated in a 24-well plate in the presence or absence of IL-23 (50 ng/ml), IL-1b (50 ng/ml), IL-6 (100 ng/ml) and TGF-β (1 ng/ml). Where indicated, LAT-1 inhibitor BCH (50 mM) or CH-223191 (3 μM) were also added to the cultures. At d2, IL-2 (100 U/ml) was added and cells were analyzed for IL-22 production at d4 of culture. First, PBMCs were incubated with human PercP-anti-Vδ2 (Biolegend) during 30 min at 4 °C, then cells were fixed (PFA 2% 10 min TA) and incubated in saponin (0.3% 10 min TA) before incubation with APC anti-human IL-22 (eBioscience). Cells were analyzed in a FACSCanto flow cytometer. Dead cell were excluded using fixable viability staining 510 (BD Biosciences). IL-22 secretion was quantified in the supernatant using Human IL-22 Ready-Set-Go ELISA kit (eBioscience).

Immunofluorescence staining and *in situ* proximity ligation assay (PLA). Frozen sections of human skin biopsies were fixed in cold acetone and blocked in PBS containing 5% of donkey serum and 100 mM/ml human γ-globulin (Sigma-Aldrich, St Louis, MO, USA). Sections were incubated with the following anti-human primary Abs (**Supplementary Table 2**): mouse monoclonal anti-CD69 (TP1.55), rabbit polyclonal anti-IL-22 (Bios, Mass USA) and goat anti-TCR-γ9 (Santa Cruz Biotechnology) for 1 h. The secondary Abs used were: AlexaFluor 488-conjugated donkey anti-rabbit, AlexaFluor 568-conjugated donkey anti-goat and AlexaFluor 647-conjugated donkey anti-mouse. Nuclei were counterstained with DAPI. Immunofluorescence pictures were taken using a Zeiss LSM Confocal microscope and analyzed with LSM image browser software.

J77 Jurkat cells or CD69-stable overexpressing J77 Jurkat cells were fixed in ice-cold methanol at -20 °C for 10 min and blocked with 1% BSA and 10% donkey serum in PBS for 2 h at room temperature. Then cells were incubated with mouse anti human CD69 mAb (TP1/55), Rabbit anti human LAT1 (Cell Signaling) or rabbit anti human CD98 (Santa Cruz) for 1 h at 37 °C (antibodies, **Supplementary Table 2**). Secondary antibodies from donkey species (**Supplementary Table 2**) or PLA detection kit reagents (SIGMA) were added for visualization of co-localization or proximity assay of these molecules in the membrane. For each duolink pair confocal microphotographs quantification of red dots per cells was conducted using Imaris Software.

Amino acid uptake assay. Naive CD4$^+$ T cells obtained from CD69-deficient and wild-type mice were cultured (1×10^6 cells/ml) in RPMI medium for 24 h, in the presence of anti-CD3 (5 μg/ml) and anti-CD28 (2 μg/ml) (**Supplementary Table 2**). Similarly, spleen/lymph-nodes γδ T cells were sorted as CD27$^+$ and CD27$^-$ and stimulated for 24 h with IL-23 (10 ng/ml) and IL-1β (10 ng/ml) in RPMI medium (1×10^5 cells/ml). ^{3}H-radiolabeled L-Trp, L-Phe and L-Leu (PerkinElmer) were added (0.5 μCi/ml) in HBSS (GIBCO) with a final extracellular L-Leu concentration of 5 μM. Amino acid uptake was measured at 5, 10, 15 and 20 min at 37 °C. Uptake was stopped by the addition of 20 mM cold L-Leu to quench System L. For the purpose of kinetic analysis, uptake at 5-min was defined as the initial uptake rate and data were analyzed only at the time interval where incorporation was linear. At the end of the assay period, cells were harvested onto glass-fiber filters using a Tomtec 96-well parallel harvester and washed vigorously for 30 s with PBS solution. β-radioactivity was counted in a Beckman LS 6500 Multi-Purpose Scintillation Counter (Beckman Coulter). Nonspecific binding of radioactivity to the filters (based on wells containing radiolabeled substrate without cells) was typically <10% of the total signal and was subtracted from each data point. Five replicates were assessed for each data point.

CD69 internalization assay. Plasmid for LAT1-mCherry expression was provided by D. Rotin(University of Toronto, USA). CD69-eGFP plasmid has been generated in our lab. HEK 293 cells maintained in Dulbecco's Modified Eagle Medium (DMEM) supplemented with 4 mM L-glutamine and 10% FBS were transfected with plasmids expressing LAT1-mCherry and CD69-eGFP using Lipofectamine Reagent (ThermoFisher). Mouse anti human CD69 monoclonal antibody (TP1/55; **Supplementary Table 2**) was directly labeled with Zenon Alexa-647 labeling Kit (Life Technologies) and incubated for 30 min with transfected cells at 37 °C. Cells were washed with PBS and fixed with 1% paraformaldehyde. Immunofluorescence pictures were taken using a Zeiss LSM Confocal microscope and analyzed with LSM image browser software.

Proteomic study design and in-gel protein digestion. For the proteomics assay, naive CD4$^+$ T cells obtained from CD69-deficient and wild-type mice were activated with PMA (50 ng/ml) plus ionomycin (750 ng/ml) for 18 h. After assessing CD69 expression by flow cytometry in wild-type cells, about 5×10^6 whole cells were incubated with hamster anti-mouse CD69 mAb (clone: H1. 2F3, Abcam) and isotype-matched control mAb (hamster anti-mouse CD31, clone 2H8, AbD Serotec) (**Supplementary Table 2**), already immobilized in Dynabeads Protein G (Life Technologies), in serum-free RPMI medium, for 1 h at 4 °C. Thereafter, cells were lysed in ice-cold 1% CHAPS lysis buffer containing 1 mM $CaCl_2$ and protease inhibitor cocktail (Complete, Roche) for 1 h at 4 °C. Magnetic separation of beads allows collecting proteins associated to CD69 and consecutive washes with ice-cold lysis buffer for 4 h for reduction of nonspecific interactions.

Proteins were digested in the gel using the following protocol. 15 μl of beads were resuspended in 30 μl of sample buffer and loaded into SDS-PAGE gel. The run was stopped as soon as the front entered 2 mm into the resolving gel. The protein band was excised and digested with 20 ng/μl trypsin at 10:1 protein: trypsin (w/w) ratio. The resulting peptides were desalted onto C18 OMIX tips (Agilent Technologies) before LC-MS/MS analysis.

Mass spectrometry. Analyses were performed using a nano-HPLC Easy nLC 1000 coupled to a linear ion trap-Orbitrap Elite hybrid mass spectrometer (Thermo Scientific). Peptides samples were loaded onto a home-made C18 reversed-phase (RP) nano-column (100 μm I.D., 45 cm) and separated in

doi:10.1038/ni.3504

a continuous gradient consisting of 8–35% B for 20 min and 35–90% B for 2 min (B = 90% acetonitrile, 0.1% formic acid) at 300 nL/min. A Picotip emitter nanospray needle (New Objective) was used for peptide ionization. An enhanced FT-resolution spectrum in the mass range of m/z 390–1,600 followed by data-dependent MS/MS spectra of the 20 most intense parent ions were acquired along the chromatographic run. Normalized CID collision energy was set to 35% and a 2-Da of parent ion mass isolation width.

Peptide identification and statistics. Peptide identification from MS/MS spectra was done using Sequest running under Proteome Discoverer 1.4 (Thermo Scientific), allowing two missed cleavages, and using 800 ppm and 0.02 ppm precursor and fragment mass tolerances, respectively. Met oxidation and Cys carbamydomethylation were selected as dynamic modifications. The MS/MS raw files were searched against the Human Uniprot database (March 2013) and results were analyzed using the probability ratio method. Post-search result filtering by mass error was done as described. For each scan, if the mass deviation fell outside the ± 5 ppm window, the corresponding XCorr was rescored to 0, whereas the pRatio was reassigned a value of 2. The false-discovery rate (1% FDR) was estimated from the search results against a decoy database.

Co-immunoprecipitation and immunoblot analysis. A human-Jurkat-cell-derived T cell line (J77) activated with PMA (50 ng/ml) and Ionomycin (500 ng/ml) for 18 h was used for co-immunoprecipitation experiments. The following mouse anti human mAbs generated in the laboratory were used (**Supplementary Table 2**): anti-CD69 (TP1/8), anti-CD98 (FG1/8), and anti-CD13 (Tea1/8) as negative control, using the same protocol and lysis buffer described for the proteomic assay. Co-immunoprecipitated proteins were separated by SDS-PAGE and immunoblotted with the following rabbit polyclonal anti human Abs (**Supplementary Table 2**): anti-CD69 (Abcam) and anti-CD98 (Santa Cruz Biotechnology). Anti-human LAT1 antiserum was provided by P. Taylor (Dundee, UK).

Immunoblot analysis of mTORC signaling was conducted with *in vitro* cultured T_H17 cells from CD69-deficient and wild-type mice. After the lysis with RIPA buffer supplemented with protease and phosphatase inhibitor cocktails (Roche), the lysates were separated by SDS-PAGE and immunoblotted with the following rabbit Abs (**Supplementary Table 2**): antibody to mTORC1 phosphorylated at Ser2448, antibody to total mTORC1, antibody to S6 phosphorylated at Ser235 and Ser236, antibody to total S6, antibody to 4E-BP1 phosphorylated at Thr37 and Thr46, and antibody to total 4E-BP1 (Cell Signaling). Control of protein quantity was assessed with rabbit anti mouse β actin antibody (Santa Cruz; **Supplementary Table 2**). All primary antibodies were detected with HRP conjugated goat anti-rabbit (Pierce; **Supplementary Table 2**). Protein bands were analyzed using the LAS-3000 CCD system and Image Gauge 3.4 (Fuji Photo Film Co., Tokyo, Japan).

Treatment of samples for L-Trp and FICZ quantification. Three biological replicates of 50×10^6 Jurkat T cells were incubated in RPMI 1640 medium w/o amino acids (US Biological Life Sciences) supplemented with 5% FCS, 2 mM L-glutamine, 100 U/ml penicillin 100 µg/ml streptomycin, non-essential amino acids (Hyclone) and L-Trp (50 mg/ml), and were treated or not with BCH (50 mM) for 24 h. The cell pellets were thawed on ice and subjected to three freeze–thaw cycles for complete cell disruption, protein precipitation and metabolite extraction. Samples were suspended in 100 µL mixture composed by MeOH:MTBE (1:1 v/v), vortex-mixed, placed in liquid nitrogen for 10 s and thaw in an ice bath (for 10 s) three times. Samples were then sonicated for 6 min and vortex-mixed for 1 min. The entire protocol was repeated three times. Subsequently samples were centrifuge at 18,000*g* for 20 min at 10 °C and the supernatants were collected (extract A) and stored at –20 °C. The residual cell pellets were extracted again with 100 µL of MeOH:MTBE (1:1 v/v), following the same procedure. Supernatants were collected after centrifugation (extract B) and the two extracts were combined.

Cell culture medium samples were thaw on ice and vortex-mixed few seconds. Then, 300 µL of MeOH:MTBE (1:1 v/v), were added to 100 µL of sample, vortex-mixed and incubated on ice for 20 min. Supernatants were collected by centrifugation at 18000*g* for 20 min at 4 °C. Finally, cells and media extracts were diluted 1:5 (for analysis of FICZ) and 1:1,000 (for the analysis of Trp) with acetonitrile:water (10:90 v/v) containing 0.1% of formic acid. Samples were vortex-mixed, centrifuged at 18,000*g* for 10 min at 10 °C to allow particle precipitation and transfer in a HPLC glass vial with 300 µL insert.

Liquid chromatography–mass spectrometry determination of FICZ and L-Trp. LC-MS grade water, formic acid, acetonitrile, and HPLC grade methyl tert-butyl ether (MTBE) and Tryptophan (Trp) were purchased from Sigma-Aldrich. Methanol (MeOH), was purchased form Fischer Chemical and formylindolo (3,2-b)carbazole (FICZ) from Enzo Life Science.

High-resolution parallel reaction monitoring (PRM) of FICZ and Trp were carried out on an Easy-nLC 1000 nano HPLC (Thermo Scientific, Waltham, Massachusetts, USA) coupled to a trihybrid quadrupole-linear ion trap-orbitrap mass spectrometer (Orbitrap Fusion Tribrid, Thermo Scientific) operating in positive polarity mode. A volume of 10 µL of diluted extracts were loaded onto an Easy-Spray (Thermo Scientific) C-18 reversed-phase nano-column (75 µm I.D., 50 cm) and metabolites were separated with mobile phase composed by A) water with 0.1% of formic acid and B) acetonitrile:water (90:10 v/v) with 0.1% of formic acid, at 200 nL/min and 50 °C. For analysis of FICZ, the gradient started at 35% B to 100% B in 10 min, holding 100% B for 12 min and returned to starting condition in 2 min, keeping the re-equilibration time for 30 min. For analysis of Trp, the gradient started at 35% B to 100% B in 15 min, holding 100% B for 9 min and returned to starting condition in 2 min, keeping the re-equilibration time for 30 min.

Metabolites were monitored by targeting the corresponding [M+H]+ ions to acquire complete MS2 spectra. Precursor ion of the FICZ and Trp (corresponding to m/z 285.10224 and 205.09715, respectively) were isolated by the quadrupole analyzer and targeted for higher-energy collisional dissociation (HCD). HCD collision energy was optimized for each compound and fragments were detected with 15000 resolution in orbitrap. Targeted parameters included a 3 Thompson isolation window around the m/z values of interest, 2.7 kV spray voltage and 310 °C as capillary temperature. Data analysis was performed with Xcalibur 2.2 (Thermo Scientific).

Statistical analysis. After analysis of data distribution with Kolmogorov Smirnov test, the statistical significance was assessed by one-tailed unpaired Student's *t*-test, one-way ANOVA with Newman-Keuls multiple-comparisons *t*-test or two-way ANOVA with Bonferroni's multiple-comparisons post-test, as required. For kinetic assay of amino acid uptake, a linear regression with slopes comparison was conducted. All analysis was performed with GrapPhad software. Differences were considered significant at $P < 0.05$.

48. Mukai, M. & Tischkau, S.A. Effects of tryptophan photoproducts in the circadian timing system: searching for a physiological role for aryl hydrocarbon receptor. *Toxicol. Sci.* **95**, 172–181 (2007).
49. Kondo, M. *et al.* Expansion of human peripheral blood gammadelta T cells using zoledronate. *JoVE* **55**, 3152 (2011).